IEEE Access
Multidisciplinary ⋮ Rapid Review ⋮ Open Access Journal

Received 2 June 2025, accepted 2 July 2025, date of publication 10 July 2025, date of current version 16 July 2025.

*Digital Object Identifier 10.1109/ACCESS.2025.3586151*

SURVEY

# Isolated Multi-Port DC-DC Converters for Renewable Energy Sources: A Review

**ALIREZA ASADI[1], XIAODONG LIANG[1], (Senior Member, IEEE), SOBHAN SARANI[1], AND MOHAMMAD SALEH KARIMZADEH[2]**

[1]Department of Electrical and Computer Engineering, University of Saskatchewan, Saskatoon, SK S7N 5A9, Canada
[2]Department of Electrical Engineering, Amirkabir University of Technology (Tehran Polytechnic), Tehran 15916-34311, Iran

Corresponding author: Xiaodong Liang (xil659@mail.usask.ca)

This work was supported in part by U.S.-Canada Center on Climate-Resilient Western Interconnected Grid, the Natural Sciences and Engineering Research Council of Canada (NSERC).

**ABSTRACT** Multi-port DC-DC converters (MPCs) become increasingly popular in power conversion for renewable energy sources (RESs), battery storage systems (BSSs), and electric vehicles (EVs). MPCs can be categorized into isolated or non-isolated structures. Isolated MPCs (IMPCs) have the galvanic isolation, higher voltage gain, bidirectional capability, and are easier to operate under soft-switching. This paper comprehensively reviews IMPCs to assist in developing new converters. Based on isolation of all or some of the ports, IMPCs can be divided into two groups: partially isolated converters (PICs) and fully isolated converters (FICs). A comparison of their architectures and features, including the applications, component count and efficiency, is presented, along with the circuit selection of IMPCs for different applications. Future research directions in IMPCs are recommended in this paper.

**INDEX TERMS** Multi-port dc-dc converters (MPCs), partially isolated, fully-isolated, half-bridge, full bridge, renewable energy sources, topology review.

## I. INTRODUCTION

With growing needs of integrating renewable energy sources (RESs), such as photovoltaics (PVs), wind turbines, and full cells (FCs), along with battery storage systems (BSSs), in power grids, efficient and reliable power conversion becomes increasingly important [1] (Fig. 1). One of the common configurations is to connect several DC sources to DC-DC converters, which can provide a constant output voltage at the load through a proper controller. Although single-input, single-output (SISO) DC-DC converters are simple in design, they increase the count and cost of components, and reduce the overall efficiency [2], [3]. Multi-port DC-DC converters (MPCs) are promising by integrating different energy sources and loads, while achieving the galvanic isolation and bidirectional power flow [4]. MPCs offer a compact and integrated solution by combining multiple input and output ports within a single converter unit, reduce the component count, cost and volume, increase the efficiency, and simplify the power management and energy transfer among the connected sources and the load.

MPCs can be broadly classified into two main categories: non-isolated MPCs [5], [6], [7], [8], [9], [10], [11] and isolated MPCs (IMPCs) [12], [13], [14], [15], [16], [17], [18], [19], [20], [21], [22], [23], [24], [25], [26], [27], [28], [29], [30], [31], [32], [33], [34], [35], [36], [37], [38], [39], [40], [41], [42], [43], [44], [45], [46], [47], [48], [49], [50], [51], [52], [53], [54], [55], [56], [57], [58], [59], [60], [61], [62], [63], [64], [65], [66], [67], [68], [69], [70], [71], [72], [73], [74], [75], [76], [77], [78], [79], [80], [81], [82], [83]. Without the galvanic isolation, non-isolated MPCs have a simpler design with a lower number of components in most structures. However, to match the voltage of the power grid/load with RESs, a high voltage gain multi-input DC-DC converter [84], [85] with a complex non-isolated topology is needed. Isolation between input sources and the load is crucial in certain applications. IMPCs can provide isolation for some or all ports, and obtain a high voltage gain by using transformers without a complex structure.

The associate editor coordinating the review of this manuscript and approving it for publication was Zhilei Yao.

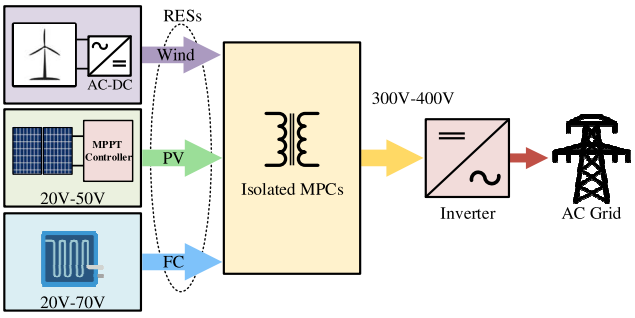


**FIGURE 1.** General overview of IMPCs for RESs.

According to Fig. 2, IMPCs can be classified into two categories: 1) partially isolated converters (PICs) by providing partial galvanic isolation between specific ports [12], [13], [14], [15], [16], [17], [18], [19], [20], [21], [22], [23], [24], [25], [26], [27], [28], [29], [30], [31], [32], [33], [34], [35], [36], [37], [38], [39], [40], [41], [42], [43], [44], [45], [46], [47], [48], [49], [50], [51], [52], [53], [54], [55], [56]; 2) fully isolated converters (FICs) by providing complete isolation between all input and output ports [57], [58], [59], [60], [61], [62], [63], [64], [65], [66], [67], [68], [69], [70], [71], [72], [73], [74], [75], [76], [77], [78], [79], [80], [81], [82], [83], meeting the safety consideration, noise immunity, and voltage level compatibility. FICs are further divided into half-bridge-based and full-bridge-based topologies. The full-bridge-based FICs include variants, such as the triple active bridge (TAB), dual-transformer TAB (DT-ATAB), interleaved TAB, other multi-port configurations, and resonant converters. PICs, on the other hand, are also classified based on their primary-side structure into half-bridge-based, full-bridge-based, and other types. For full-bridge-based PICs, different input-module combinations (Module-1 to Module-4) are used to define how energy sources are interfaced with the primary side of the converter.

PICs have been popular for a long time due to their capability of combining non-isolated and isolated circuitries in a single converter topology to achieve power conversion between directly connected sources and energy storage, while offering isolation and voltage adaptation to the load [34], [38]. Compared to FICs, PICs offer a higher power density and efficiency with soft-switching, fewer components, lower cost and volume [86]. FICs offer the complete galvanic isolation between all ports, often use multi-winding transformers or multi-two-winding transformers to isolate each port, and achieve higher safety and noise immunity, but at the expense of the added complexity, a higher manufacturing cost, and a larger volume [75].

PICs and FICs can be further categorized into half-bridge-based (HBB) and full-bridge-based (FBB) according to the structure of the primary side of their transformer. HBB converters have been very popular because of their simplicity, the lower component count, and ease of handling a wide range of input voltage, suitable for integrating energy storage, such as batteries and ultra-capacitors. FBB converters handle higher power levels, and provide better voltage stress distribution across switches and efficient bidirectional power flow, suitable for industrial and high-power applications.

IMPCs use soft switching for switches, which reduces circulating currents and conduction losses, and decoupled control for independent power flow. Different topologies and control techniques have been proposed in the literature to improve the efficiency, and reduce electromagnetic interference (EMI).

In several review papers [1], [85], [103], [104], different multi-port converter topologies are compared. However, the lack of comprehensive consideration of IMPCs in these papers motivates the authors to review IMPCs thoroughly. In [86], different types of current-fed isolated bidirectional DC-DC converters are reviewed, but multi-port structures are not covered. Another significant contribution of this paper is that it explicitly explains the difference between the partial and fully isolated topologies and reviews the most recent and impactful studies, which has not been done in previous review papers. This review paper presents recent advances in IMPCs by classifying various converter architectures, analyzing their advantages and disadvantages, presenting the design considerations, control strategies, resiliency, and performance metrics, and providing guidelines for selecting the most suitable topology.

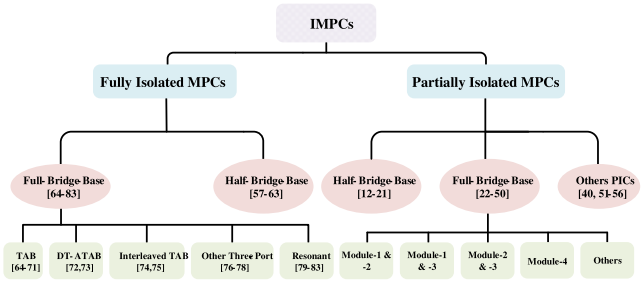


**FIGURE 2.** Overview of multi-port isolated DC-DC converters.

## II. PARTIALLY ISOLATED CONVERTERS

PICs offer a hybrid advantage from non-isolated and fully isolated topologies, and maintain compact designs and a high-power density. One limitation of PICs is that only a narrower voltage range can be provided compared to FICs. In PICs, isolation can occur between the input sources and the output (Fig. 3(a)), or between one of the input sources and other input ports (Fig. 3(b)). Load-isolated PICs (Fig. 3(a)) have been studied extensively. Partly-isolated three-port converters generally involve two directly connected ports, which are linked to the third port via the galvanic isolation. While some output and bidirectional inputs are connected without isolation, they are connected to the input port through a high frequency transformer (Fig. 3 (b)).

The primary structure of PICs integrates non-isolated buck, boost, interleaved, or buck-boost circuits into the primary-side circuit of isolated converters, such as

half-bridge converter (HBC) and full-bridge converter (FBC). IMPCs in use today include the isolated FBC with four controllable power switches for each source, the isolated HBC with two switches per source, and the isolated single-switch converter with one switch per source. In this paper, PICs are categorized into three types based on the primary side of the transformer: half-bridge-based (HBB) [12], [13], [14], [15], [16], [17], [18], [19], [20], [21], full-bridge-based (FBB) [22], [23], [24], [25], [26], [27], [28], [29], [30], [31], [32], [33], [34], [35], [36], [37], [38], [39], [40], [41], [42], [43], [44], [45], [46], [47], [48], [49], [50], and other PICs [40], [51], [52], [53], [54], [55], [56].

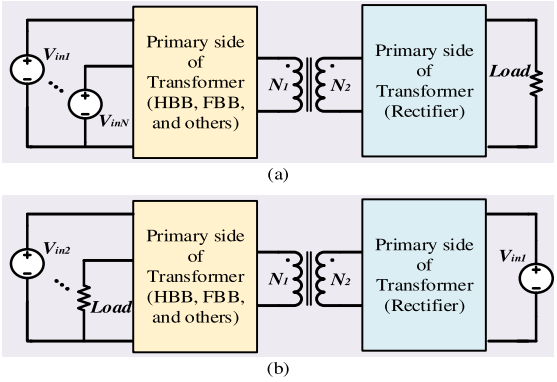


**FIGURE 3. Main architectures for PICs with three ports: (a) Isolation between input and output, (b) Only one input isolated [21].**

### A. HALF-BRIDGE-BASED PICS

The half-bridge-base PIC (HBB-PIC) is a fundamental isolated topology, and its switches on the primary side operate alternately/complementarily. The switch leg is in parallel with the capacitor branch of the HBC, as shown in Fig. 4(a). Each switch and its corresponding capacitor function as the active clamp for its complementary counterpart. Within the HBC, the input capacitors act as multi-purpose voltage sources, facilitating both increase and decrease of the voltage, which sets the stage for constructing a MPC derived from a HBC structure. The HBC structure in multi-port PICs brings three key advantages: minimizing switching losses to increase the efficiency, a lower component count to ensure cost-effectiveness and simplicity, and the precise voltage regulation essential to manage multi-output ports. This simplicity improves the system reliability by using fewer components, making maintenance and control easier. It also offers scalability and adaptability to different power levels, and better thermal management due to the reduced heat dissipation, and thus, it is proven to be an efficient power conversion solution in various applications [15], [16], [17].

Fig. 4(b) shows the topology of [12], [13], and [14], where a converter uses both the DC link and magnetic coupling to connect and control three separate voltage buses. The topology in [12] combines a bidirectional boost converter with a HBC, and the energy moves from the PV port to the load through a magnetic coupling via the DC link. In this topology, the battery can be charged only when its voltage is lower than that of the PV port. The topology in [13] features a direct connection of the battery port to the midpoint of the DC-link capacitor leg, but the average battery current passes through the transformer's magnetizing inductance, causing a DC flux bias within the transformer and increasing power losses. Reference [14] designs a three-port HBC (TPHBC) by focusing on the power flow analysis among the ports and precise control of power transmission.

TPHBC converters can be classified into three categories: 1) with post-regulation, 2) with synchronous regulation (SR), and 3) with primary freewheeling. TPHBCs with post-regulation in [12] and [13] have the same primary side and a different setup on the secondary side. Both primary switches in the post-regulation stage can be operated with zero-voltage switching (ZVS), leading to reduced power losses in the primary circuit compared to other TPHBC topologies. However, a post-regulation switch with added conduction losses on the secondary side may not be the best choice for high load current applications. TPHBC with synchronous regulation stands out for its minimal component count; they are suitable for applications requiring low output voltage and high current, but not suitable for high output voltage applications due to the reverse recovery loss impacting switches and in Fig. 4(b). All active switches, except, operate with ZVS, i.e., the primary switching losses in TPHBC-SR tend to be higher than that in other TPHBC variants [14]. With two switches in the secondary side of the transformer for synchronous regulation, it's possible to independently regulate the voltage of the three ports. By replacing synchronous regulation with post-regulation in the converter, several other converters can be derived [14]. These derived converters offer reduced component numbers and simpler configurations. Their efficiency remains relatively high as the power flow between any two of the three ports occurs in a single stage.

The design in [15], [16], and [17] is built upon both HBC in Figs. 4(b) and 4(c) with an extra switch and a diode on the primary side of the transformer, initially introduced in [15]. Adding this free-wheeling branch across the transformer with the leakage inductor () during the OFF state of both and introduces an extra controllable branch, resulting in a tri-modal half-bridge topology to achieve ZVS for all switches. However, this leads to a more complex topology and additional conduction losses than the converter in Fig. 4(b). This concept is expanded in [16] and [17] by incorporating a time-sharing approach into the proposed integrated multiport topology. In [17], the primary side of the converter features three ports: two sources and one bidirectional storage port. The secondary side in [16], [17] is enhanced over [15] by implementing synchronous rectification to minimize conduction losses and using two switches to replace the diode at the output port. ZVS can also be achieved for all three primary switches (, , and ) in Fig. 4(c). The tri-modal converter in [15] displays structural resemblances with the ZVS duty-cycle

**TABLE 1. Summary of HBB-PICs.**

| HBB-PICs | No. of Inputs | No. of Outputs | Power (W) | Frequency (kHz) | No. of Components | | | | | ZCS | ZVS | Voltage Gain | Target Applications | Disadvantages |
|---|---|---|---|---|---|---|---|---|---|---|---|---|---|---|
| | | | | | D | S | C | I | T | | | | | |
| [12] | 3 | 1 | 2000 | 40 | 0 | 4 | 5 | 1 | 10 | No | Not All | $nD$ | Electric vehicles (EVs) | - High switching losses<br>- Load dependent operation |
| [13] | 3 | 1 | 1400 | 22 | 0 | 4 | 4 | 0 | 8 | No | All | $nD$ | EVs | - Each output cannot be controlled independently |
| [14] | 2 | 1 | 120 | 100 | 1 | 4 | 3 | 1 | 9 | Yes | All | $nD$ | Hybrid energy systems (HES) | - Load dependent soft-switching operation |
| [15] | 2 | 1 | 200 | 100 | 3 | 3 | 3 | 1 | 10 | No | All | $2n(d_{12}-\delta)$ | HES | - Non-continuous input current |
| [16] | 2 | 1 | 200 | 100 | 1 | 5 | 3 | 1 | 10 | No | All | $2nD$ | Satellite power systems | - High control complexity |
| [17] | 3 | 1 | 39.6 | 100 | 2 | 6 | 4 | 1 | 13 | No | All | PSM | HES | - High cost and control complexity |
| [18] | 3 | 1 | 1000 | 100 | 4 | 4 | 4 | 1 | 13 | No | Not All | $2n(d_{12}-\delta)$ | HES | - High switching losses and cost |
| [19] | 2 | 1 | 400 | 100 | 6 | 4 | 3 | 1 | 14 | No | All | $N(\frac{\varphi}{2\pi}2D(1-D))$ | HES | - High cost and control complexity |
| [20] | 2 | 1 | 250 | 100 | 0 | 4 | 5 | 2 | 11 | No | All | $nD$ | HES | - High volume |
| [21] | 2 | 1 | 1500 | 100 | 3 | 3 | 5 | 3 | 14 | Yes | No | $(1+\frac{N_4}{N_3}\frac{V_{bat}}{V_{in}})d_1\frac{N_2}{N_1}$ | HES | - High control complexity and volume |

Note: In this table, parameters D, S, C, I, and T represent the number of diodes, switches, capacitors, inductors, and total count of components.

shift-controlled symmetric half-bridge (DCS-HB) converter in [17]. The main difference is that the DCS-HB topology operates as a two-port system with primary switches and, The main difference is that the DCS-HB topology operates as a two-port system with primary switches and, working at the same duty cycles, while the tri-modal topology handles duty cycles of these switches independently to manage the additional bidirectional port. This results in an asymmetrical operational mode and design adjustments, but maintains ZVS.

There are several half-bridge-based PICs proposed in [18], [19], [20], and [21]. In [18], the H-bridge configuration from [37] is split into two half-bridge topologies on the primary side while sharing the battery port, resulting in a new converter with four ports (Fig. 5(a)). The secondary side incorporates a full-bridge rectifier.

Various MPCs are proposed for RESs integration into power grids, but active switches are excessively used, and the battery's lifespan is negatively affected due to high frequency charging and discharging cycles in a single switching period [18]. Most existing MPCs have only three ports. The converter in [19] merges two parallel half-bridges into an interleaved half-bridge, three-port converter for RESs (Fig. 5(b)). The primary side circuits operate in parallel, while the secondary windings run in series, sharing a common rectification and filter setup. It forms three full-bridge diode rectifiers, with Leg-1 and Leg-2 creating a full-bridge rectifier for an equivalent FBC made from the two HBCs. This arrangement eliminates the freewheeling stage, and conduction losses due to circulating currents in conventional full-bridge converters (FBC). It extends the voltage gain and

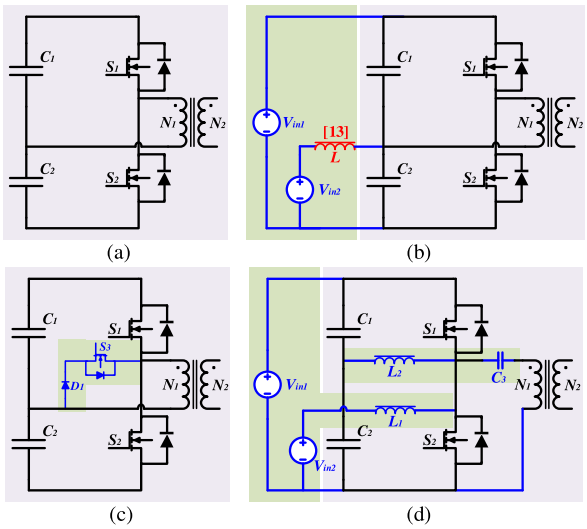


**FIGURE 4. Different topologies for PICs, based on the half-bridge. (a) primary side of HBC. (b) a bidirectional buck-boost converter with a half-bridge converter [12], [13], [14]. (c) Tri-modal HBC. [15], [16], [17]. (d) HBC in [20].**

reduces output filter requirements. In [20], a HBB-PIC operating at 1 MHz is introduced (Fig. 4(d)), featuring a compact planar high-frequency transformer, which reduces the volume and efficiently handles three distinct DC voltages, and results in a high voltage gain. All four switches have ZVS capability, enhancing its efficiency. The converter operates with a simple switching pattern and a nonlinear digital control scheme adaptable across all duty cycle ranges. Despite its small size, it maintains a high efficiency and power density, and includes

a bidirectional converter interfaced with the battery, and a unidirectional converter for PV systems. In contrast to prior converters, [21] features a single port on its primary side, with a solitary battery source and a load on the secondary side. It combines the half-bridge (Fig. 4(a)) with a boost topology (Fig. 5(c)) and includes an extra capacitor on the primary side for zero-current switching (ZCS). The input magnetic switching boost section continuously conducts current from the PV array, while elevating the input voltage, which forms an energy-balancing unit with a boost component, spurring new single-module and parallel control methods. This setup enables ZCS for all primary diodes and MOSFETs, enhancing efficiency and compactness. Efficient battery charging is managed by controlling the input current of the boost stage, positioning the boost converter as an energy-balancing component.

*Summary of HBB-PICs*: Table 1 summarizes the component count, rated power, and efficiency at the rated power for HBB-PICs. All converters have a step-down voltage gain. The proposed converters in [12], [13], [14], and [20] are based on the conventional HBB and have the lowest step- down capability. The converter in [15] effectively doubles the gain and incorporates the modulation margin ($\delta$) to enable a broader control, a feature also seen in [18]. Reference [19] introduces a more complex gain expression, blending the phase shift ($\varphi$) and the duty-based quadratic control to extend the regulation flexibility. One degree of freedom is added in [21] by incorporating two turn ratios into the voltage gain. However, the control complexity increases since the voltage ratio of the battery and PV source should be determined. Despite the voltage gain that each converter can provide, the converters in [12] and [18] suffer from high switching losses, as soft-switching is not used for these converters. Additionally, [12] exhibits load-dependent operation characteristics, i.e., the performance and regulation quality can vary based on load conditions. Reference [13] shares a similar drawback, and each output cannot be controlled independently. Although the converter in [14] offers soft-switching, its operation is constrained by load-dependent ZVS. The HBB-PIC in [15] has a non-continuous input current, which can increase the input filter and decrease the lifespan of input sources [105], [106], [107]. The converters in [16], [17], and [19] suffer from high cost and control complexity, due to a high number of total components and switches. The highest number of passive components is utilized in [20] and [21], which increases the volume of the converter. Notably, most HBB-PICs are to be utilized in hybrid energy systems (HESs).

In HBB-PICs, soft-switching is generally achieved through resonant transition techniques or parasitic energy recycling. References [15], [16], [18], and [19] utilize leakage inductance of the coupled inductors and switch's parasitic capacitance to enable soft-switching. In [16], ZCS is achieved for secondary-side diodes through the controlled resonant current formation, while switches on the primary side benefit from quasi-ZVS turn-off by utilizing leakage inductance and appropriate dead-time between switching. To extend the soft-switching range, the studies in [13], [15], and [20] utilize resonant snubbers or magnetic coupling along with modulation strategies, such as interleaved PWM or adaptive dead-time control. Overall, in these studies, soft-switching is achieved by passive elements. Therefore, maintaining soft-switching across a wide operating range requires accurate component design.

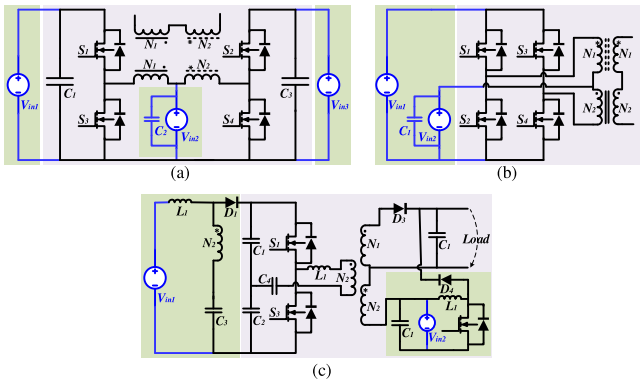


**FIGURE 5.** HBB-PICs. (a) [18], (b) [19], (c) [21].

### B. FULL-BRIDGE-BASED PICS

The Full-Bridge-Based PICs (FBB-PICs) are robust and adaptable. Using a minimum of two legs and four switches, they enable bidirectional power flow, and handle higher power than HBB-PICs. FBC offers a higher efficiency, the reduced voltage stress on switches, the extended lifespan and reliability, and superior output voltage quality with reduced ripples due to a balanced operation. However, more semiconductors and passive components are required (the increased number of semiconductor switches also requires additional auxiliary power supplies and gate drivers), which potentially increases the system's cost and complexity in control, resulting in a larger and heavier converter than HBB-PICs. Transformer losses in FBB-PICs are not significantly different from that in HBB-PICs at the same voltage and power levels.

Similarly, FBB-PICs can also be categorized based on the primary side of the transformer. Fig. 6(a) illustrates a full-bridge cell. To add a port to a full-bridge cell, four types of inputs are considered (Figs. 6(b)-6(e)). Fig. 6(b) shows the typical full-bridge input cell (Module-1), paralleled with both full-bridge legs and optionally paralleled with a capacitor (), suitable for RESs. Fig. 6(c) shows a branch with a source and an inductor in series (Module-2), also potentially paralleled with a capacitor (), connecting to one of the middle legs of the full bridge. It can be operated in boost or buck mode with lower current ripples compared to Module-1. An interleaved buck/boost module (Module-3) is shown in Fig. 6(d), with each point connected to the middle point of the corresponding leg. Module-3 can perform in a buck or boost mode, and has all the benefits of an interleaved cell, including low current ripples. Similar to Module-1, Fig. 6(e) connects this Module

to each leg of the full-bridge separately (Module-4). These introduced branches for the primary side of the transformer form various FBB-PICs, including resonant and dual active bridge (DAB) converters. Different types of FBB-PICs are investigated below by incorporating these Modules.

Fig. 7 shows the circuits proposed in [22], [23], [24], [25], and [26], primarily relying on Module-1 and Module-2, and sharing a nearly identical topology. In [22], a FC and a super-capacitor are connected as Module-2, which is linked to different legs of the full-bridge cell due to their closely matching operating voltages, while the load is connected through a transformer winding. Six switches enable bidirectional functionality across all three ports, and support both boost and buck modes, elevating a low operating voltage at the FC and energy storage to a higher load-side voltage, such as 400 V; it is then fed into an inverter to generate an AC output. Reference [23] introduces a quasi-Z-source four-port converter integrated with a PIC architecture for PV systems and ESSs. Module-1 is for the PV input, and a quasi-Z-source influenced by Module-2 supplies the supercapacitor and battery. Using Switch S_2, the system integrates the quasi-Z-source and the full-bridge cell. This setup reduces the rated voltages of the supercapacitor and battery's inputs via the high-gain quasi-Z-source converter, and uses a high-frequency transformer (HFT) with a low turn ratio. A controlled full-wave rectifier on the HFT's secondary side enables bidirectional power flow. In [24] and [25], a similar concept for the primary side of the transformer is presented and two three-level DAB converters using diode clamping are introduced. Reference [24] aims for the single-stage power conversion between the RES and a bipolar load with two Module-2 and one Module-1 inputs, creating a five-port converter with a bipolar secondary structure. However, load imbalances require additional voltage balance control, complicating the system. In contrast, [25] uses a diode rectifier on the output and a DC-blocking capacitor to prevent the HFT saturation. While this topology allows the battery to charge from the PV, it cannot perform bidirectional power transfer due to the diode rectifier on the secondary side of the HFT. Integrating non-isolated converters, such as buck, boost, cuk, SEPIC, or zeta with full-bridge cells, creates four-port and five-port converters through Module-1 and Module-2 [26]. These configurations offer soft-switching for active switches, and decoupled control with phase shift and pulse width modulation (PWM). The secondary side includes a full-bridge rectifier for the load port.

Several configurations combining Module-3 and Module-1 are introduced in [27], [28], [29], [30], [31], [32], [33], [34], [35], [36], [37], [38], [39], [40], and [41]. In [27], [28], [29], [30], [31], [32], [33], [34], [35], and [36], the same circuit design for the primary side of the transformer is adopted (Fig. 8(a)) by incorporating two inputs. These converters offer reduced input current ripples through interleaving (Module-3), which is beneficial for ripple-sensitive power sources, and provide bidirectional ports. While multiple studies [27], [29], [30], [32], [34], [35], [36] explore various three-port

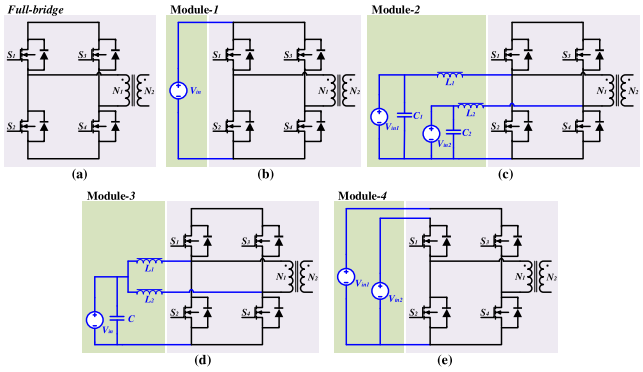


**FIGURE 6.** Different input modules for FBB-PICs. (a) basic full-bridge cell. (b) typical full-bridge input Module (Module-1) [26]. (c) a source and an inductor in series (Module-2) [22]. (d) interleaved buck/boost Module (Module-3) [27], [28], [29], [30], [31]. (e) Module-1 connected to separate legs (Module-4) [44], [45], [46], [47].

PICs, they require an additional port for interfacing more than three sources. Differences are in the design of the secondary sides and switch control methods. Control schemes vary from PWM plus phase angle shift (PWM-PPAS) control [29] to phase-shifted PWM signals, phase angle and duty cycle [35]. However, primary-side modulation and phase-shifted FBC introduce voltage and current ripples, conduction losses, and voltage spikes. To address these drawbacks, bridgeless boost rectifiers in [27] and modified modulation schemes in [32] are proposed. While some configurations employ diode rectifiers on the secondary side [27], [29], [35], others use bidirectional switches for direct connection to AC ports [30], [32], [34]. For instance, [30] includes four quadrant bidirectional switches configuration; [34] proposes a secondary active voltage six-folder rectifier to achieve a higher voltage gain and broaden the soft-switching range; [32] is based on an interleaved structure on the secondary side. These varied designs aim to improve the power control, reduce losses, widen soft-switching ranges, and eliminate circulating currents, ultimately enhancing the efficiency and broadening input voltage range of the converter [34], [36].

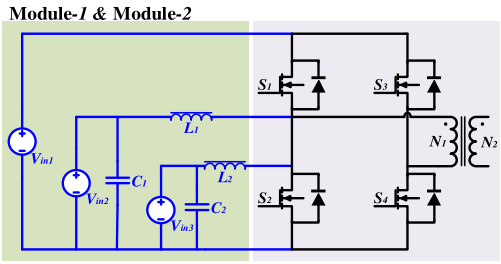


**FIGURE 7.** Primary side of FBB-PICs with Module-1 and Module-2 combinations with three sources [22], [23], [24], [25], [26].

References [28] and [31] propose a four-port DAB converter with a third input source on the secondary side connected to Module-3. The power flow between the two sides is controlled by the phase shift angle $\varphi$. In [33], a novel phase-shift modulated (PSM) buck-boost voltage balancer

is introduced by combining with a conventional full-wave rectifier, leading to a symmetrical and controlled bipolar output voltage through integration of RESs and ESSs in a bipolar DC microgrid. Module-3 and Module-1 are combined in [37], [38], [39], [40], and [41]. In [37] (Fig. 8(b)), two bidirectional buck-boost converters can be interleaved using winding-cross-coupled inductors (WCCIs) as the transformer, which reduces the component count and simplifies the magnetic structure, but it can only be used for two sources. To address this issue, [38] proposes a topology based on [37] with three sources (Fig. 8(b)). When inductors in Fig. 8(a) are coupled (Fig. 8(c)) [41], a magnetic-integrated technique is implemented to reduce the core loss and increase power density using a single core.

LLC converters [39], [40] (Fig. 8(d)) can perform buck and boost operations and achieve a high efficiency, and thus, are widely used in various applications. Reference [39] presents a three-port converter by integrating LLC resonant and buck-boost functionalities through shared active switches, soft-switching can be achieved by utilizing the duty cycle control method. Reference [40] introduces isolated four-port resonant converters with symmetrical bipolar outputs, achieving the single-stage power conversion, soft switching, and decoupled control.

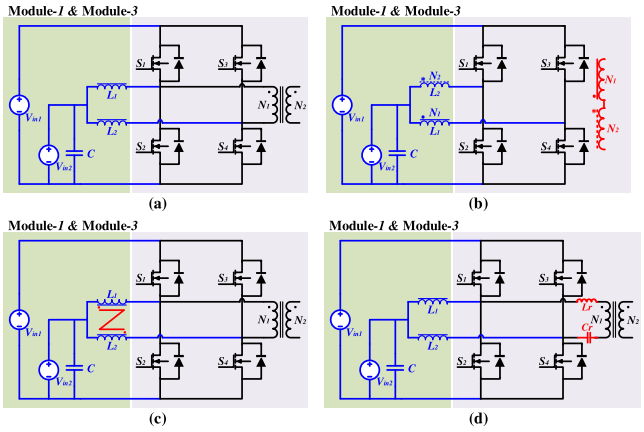


**FIGURE 8.** Primary side of FBB-PICs with Module-1 and Module-2 combinations with three sources [22], [23], [24], [25], [26].

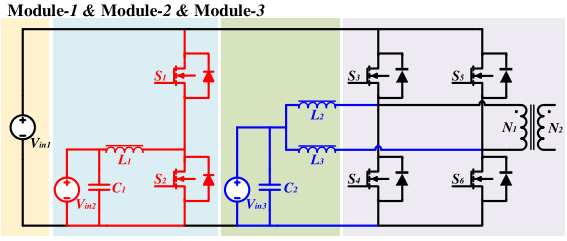


**FIGURE 9.** Primary side of FBB-PICs with Module-1, Module-2, Module-3 combinations [42], [43].

Module-2 and Module-3 are combined in [42] and [43] (Fig. 9), where a two-stage DAB converter for the ESS with time-sharing of active switches is developed in DC microgrids, offering high power density and high voltage-to-current ratio. Due to the two-stage structure of the proposed converters, it is easy to implement an independent design between the power sharing control in the storage stage, and the droop control on the output side. Consequently, multiple control loops can be implemented independently. The difference between them is that [43] has three inputs, and the extra one is implemented by Module-1.

Reference [44] introduces an approach to derive three-port PICs from a full-bridge setup involving Module-4 (Fig. 10(a)). This topology reduces device requirements and enables single-stage power conversion between any two of the three ports. The converter functions as a buck-boost converter. Bidirectional power flow among all ports is possible with bidirectional switches, but there are limitations on the output power for each port on the primary side because the power output of one port is influenced by the duty ratio of other ports. To address this issue, [45] introduces split dc-link dual-active-bridge (SDLDAB)-based PICs (Fig. 10(b)), offering a low-power alternative to three-port PICs in [46]. Unlike its predecessor, which utilized three transformers and three-leg active bridges, the topology in [46] incorporates fewer elements, yet maintains five ports. Similarly, the same concept of spilt leg is proposed in [47], in which the secondary side full-bridge rectifier can be split into two separate switching legs with a common ground and different positive terminals to obtain two dc output ports (Fig. 6(e)). The primary side can be one of the structures by combining Module-1, Module-2, and/or Module-3.

FBB-PICs in [48], [49], and [50] do not follow the Module-2, Module -3, and Module-4 framework. In [49] (Fig. 11(a)), a proposed three-port LLC resonant converter integrates two extra switches into one leg to accommodate an additional input. This converter operates using pulse-frequency modulation alongside phase-shift combined control, facilitating soft switching for nearly all switches and diodes, much like a traditional LLC resonant converter. The topology in [48] (Fig. 11(b)) features a center-tapped HFT and functions as a four-port DAB, where the transformer integrates center taps, with two coupled inductors connected between the transformer and the midpoints of each full bridge. These two full bridges establish two DC ports, while the primary and secondary connections of the HFT originate from the additional ports featuring the center taps. Reference [50] introduces a multi-input setup, featuring an isolated bidirectional DAB (Fig. 11(c)). This configuration is versatile, supporting independent or combined operation of sources to manage power transfer and enable bidirectional power flow. Operating independently reduces the circulating power and peak current stress, and enhances the efficiency of the dual active bridge converter. It also accommodates sources with unequal voltage levels by arranging them in series on the multi-input side. However, adding an additional input requires two more switches in the topology, which increases the cost and volume of the circuit.

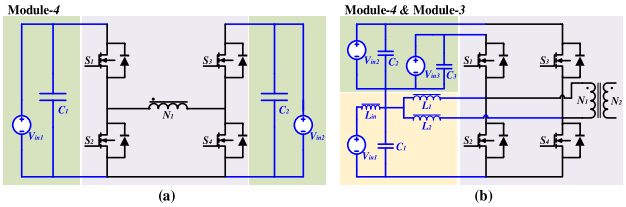


**FIGURE 10.** FBB-PICs with Module-4 combinations. (a) [44]. (b) [45].

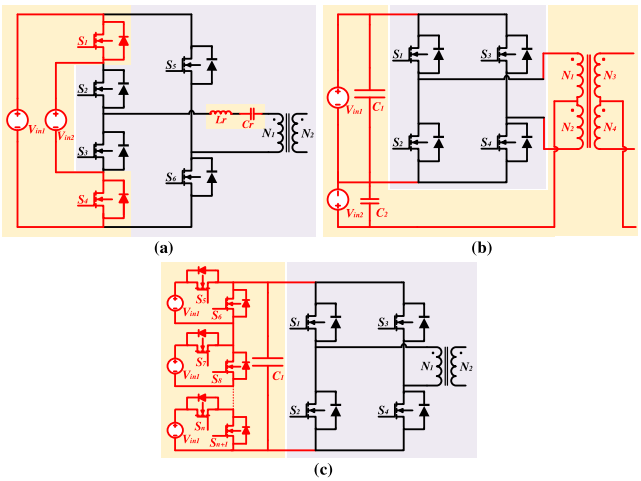


**FIGURE 11.** Other FBB-PICs. (a) [49]. (b) [48]. (c) [50].

*Summary of FBB- PICs*: Table 2 shows a comparison of FBB-PICs regarding their component count, rated power, efficiency at the rated power, etc. Notably, the table reports only the boost voltage gain equations for consistency. References [33], [35], [36], and [40] effectively balance soft switching (ZVS and ZCS), low component counts, and high efficiency. However, [46], [47], and [50] lack essential soft switching features, and have high semiconductor counts. Module-1 and Module-3 emerge as the most promising: all switches with ZVS, the moderate component count, and a higher efficiency. In contrast, Module-4 predominantly includes converters with an excessive number of semiconductors, complicated design and implementation, although they can achieve a decent efficiency. The combination of Module-1 and Module-2 shows a varied performance, some converters lack full ZVS and ZCS, but maintain a reasonable efficiency, such as [23] and [26]. The combination of Module-2 and Module-3 demonstrates a solid performance [42], [43] by offering full ZVS, moderate component counts. The group, ''Others'', in Table 2, is diverse, but generally does not outperform the combination of Module-1 and Module-3. Converters in ''Others'' often lack full soft switching features, and have higher component counts, reducing their overall appeal.

Most FBB-PICs support both buck and boost operation; however, those in [25], [29], [44], [47], and [48] are limited to unidirectional power flow. The highest boost gain appears in the converter in [34] due to its multi-stage structure and voltage multiplication circuit, making it particularly suitable for high step-up applications. In contrast, the converters in [28], [30], and [41] offer the lowest boost gains. While increasing the transformer leakage inductance in [37] helps extend the ZVS range, it also reduces the effective energy transfer to the load, thereby decreasing the achievable output voltage. The asymmetric modulation in [26] can cause DC bias in the magnetic core and increase the core losses. The unidirectional power flow, as seen in [40], [44], and [48], is a critical limitation for advanced HESs, as it prevents the grid-to-battery charging, and reduces resilience during the low-generation period. High switching loss is the main issue in the converters in [22], [23], [29], [34], [48], and [49], often due to hard-switching transitions, high switching frequencies, or insufficient soft-switching strategies. Phase-shift modulation (PSM) is the most popular control method in full-bridge-base converters. All FBB-PCIs are controlled by the PSM method, however, in some cases, like the converters proposed in [28], [30], [31], [32], [36], [43], and [45], the multi-parameter coordination, duty cycle, dual phase shift (DPS), and voltage balancing, adds to the system design and control complexity. Large volume or high component count can impact the power density and cost of the converters in [34], [48], and [50].

In [22], [23], [29], [34], [35], and [49], ZVS is achieved by proper selection of the transformer leakage inductance to ensure it forms a resonance circuit with the switch parasitic capacitance. Therefore, a proper phase alignment guarantees that current flows through body diodes before turn-on intervals of the switches. However, ZVS is load-dependent and may be lost under light load or mismatched port voltage conditions, as observed in [22], [23], and [35]. Hybrid modulation approaches, such as PWM plus phase-shift, are utilized in [27], [30], [31], and [32] to extend the ZVS range by decoupling control of power flow and switch transitions. The converters in [28], [37], and [40] utilize leakage energy to support soft-switching. However, they may require trade-offs between the ZVS range and the output voltage gain. Overall, soft-switching mostly relies on a proper design of the circuit, and can be maintained with the careful transformer design, phase modulation, or adding auxiliary circuits to enhance the soft-switching operation range. FBB-PICs in Fig. 14 and Table 3 are compared based on the number of components, bidirectional capability, current stress of semiconductors, and output gains.

### C. OTHER PICS

PICs can be categorized into half-bridge and full-bridge topologies. To take advantage of isolated ports and accommodate multiple ports, different circuits are proposed in [40], [51], [52], [53], [54], [55], and [56] (Fig. 13). MPCs are introduced by connecting various boost and buck-boost converters in parallel on the primary side of the transformer, enabling power allocation among diverse energy sources. The primary goal of [52] (Fig. 13(b)) is to achieve the simultaneous maximum power point tracking (MPPT) in a

**TABLE 2. Summary of FBB-PICs.**

| | FBB-PICs | No. of Inputs | No. of Outputs | Power (W) | Frequency (kHz) | No. of Components | | | | | ZCS | ZVS | Voltage Gain | Target Applications | Disadvantages |
|---|---|---|---|---|---|---|---|---|---|---|---|---|---|---|---|
| | | | | | | D | S | C | I | T | | | | | |
| Module-1 and Module-2 | [22] | 2 | 1 | 1000 | 100 | 0 | 6 | 5 | 2 | 13 | No | Not All | $\frac{1}{(1-D)}$ | Fuel cell | -High switching losses |
| | [23] | 3 | 1 | 10000 | 20 | 2 | 6 | 4 | 2 | 14 | No | No | $\frac{n}{(1-D)}$ | HES | -High switching losses |
| | [24] | 3 | 2 | 2500 | 20 | 4 | 12 | 4 | 2 | 22 | No | Not All | $\frac{2n}{(1-D)}$ | DC microgrid | -high cost, control complexity, and switching losses. |
| | [25] | 2 | 1 | 10000 | 20 | 4 | 4 | 4 | 2 | 14 | No | Not All | $n(\frac{\varphi}{\pi}(1.5-D)$ | HES | -High switching losses and control complexity |
| | [26] | 3 | 1 | 500 | 100 | 4 | 4 | 4 | 3 | 17 | No | All | $\frac{1}{(1-D)}$ | HES | -Asymmetric modulation |
| Module-1 and Module-3 | [27] | 2 | 1 | 500 | 100 | 2 | 6 | 4 | 2 | 14 | No | All | $\frac{V_{pv}}{2nV_o}$ | HES | -The PV port voltage needs to be pre-regulated. |
| | [28] | 3 | 1 | 10000 | 20 | 0 | 8 | 1 | 4 | 13 | No | All | PSM | HES | -Complex control method |
| | [29] | 2 | 1 | 100 | 100 | 2 | 4 | 2 | 3 | 11 | No | Not All | $\frac{2}{n}D$ | HES | -High switching losses |
| | [30] | 2 | 1 | 200 | 50 | 0 | 8 | 4 | 3 | 15 | No | All | DPS | HES | -Complex control strategy using dual phase-shift method |
| | [31] | 3 | 1 | 1000 | 25 | 0 | 10 | 3 | 4 | 17 | No | All | $\frac{n+1}{(1-D)}$ | DC microgrid | -Complex control method constrained by the ZVS condition. |
| | [32] | 2 | 1 (AC) | 200 | 50 | 0 | 10 | 3 | 4 | 17 | No | All | $\frac{n}{D}$ | HES | -Complex control method constrained by the ZVS condition. |
| | [33] | 2 | 2 | 600 | 100 | 2 | 6 | 4 | 3 | 15 | Yes | All | $\frac{1}{D}$ | Bipolar DC bus | -Load dependent soft-switching condition |
| | [34] | 2 | 1 | 500 | 100 | 4 | 6 | 8 | 2 | 20 | No | All | $\frac{6n}{D}$ | HES | -High volume |
| | [35] | 2 | 1 | 1000 | 60 | 4 | 4 | 3 | 2 | 13 | Yes | All | $\frac{n}{(1-D)}$ | HES | -Lower switches experience higher current stress than upper switches. |
| | [36] | 2 | 1 | 600 | 100 | 2 | 6 | 3 | 2 | 13 | No | All | $\frac{n}{D}$ | HES | -Only buck-mode operation is supported during CCM2. |
| | [37] | 2 | 1 | 500 | 100 | 4 | 4 | 2 | 1+1C | 12 | No | All | $\frac{1}{D}$ | HES | -Tradeoff between ZVS and output voltage range |
| | [38] | 3 | 1 | 120 | 50 | 2 | 6 | 5 | 3 | 16 | No | All | $\frac{2n}{D}$ | DC microgrid | -high circulation current at high loads |
| | [39] | 2 | 1 | 500 | 74-100 | 4 | 4 | 4 | 3 | 15 | Yes | All | $1/D$ | HES | -Load-dependent ZVS operation |
| | [40] | 2 | 2 | 500 | 100 | 4 | 6 | 4 | 2 | 16 | Yes | All | $\frac{1}{D}$ | Bipolar DC bus | -Unidirectional power flow |
| | [41] | 2 | 1 | 1000 | 50 | 0 | 8 | 1 | 1C | 10 | No | All | $1/(1-D)$ | Bidirectional applications | -Complex control methods |
| Modules -2 & -3 | [42] | 2 | 1 | 100 | 20 | 0 | 10 | 1 | 3 | 14 | No | All | PSM | DC microgrid | -ZVS condition complexity |
| | [43] | 3 | 1 | 170 | 50 | 0 | 10 | 2 | 3 | 15 | No | All | PSM | HES | -non-continuous current in PV port |
| Module-4 | [44] | 2 | 1 | 180 | 100 | 4 | 4 | 3 | 1 | 12 | No | All | $2nD$ | HES | -Unidirectional power flow and only buck operation |
| | [45] | 3 | 1 | 1000 | 15 | 0 | 8 | 4 | 3 | 15 | No | Not All | $1/(1-D)$ | HES | -High switching losses |
| | [46] | 4 | 1 | 1200 | 15 | 0 | 12 | 5 | 4 | 21 | No | Not All | $D/(1-D)$ | HES | -High volume and complex structure |
| | [47] | 2 | 1 (AC) | 1500 | 20 | 0 | 16 | 3 | 1 | 20 | No | Not All | $D$ | Bidirectional applications | -High volume and complex structure |
| Others | [48] | 2 | 2 | 1500 | 40 | 0 | 8 | 4 | 4 | 16 | No | Not All | $1-D$ | EVs | -High switching losses |
| | [49] | 2 | 1 | 500 | 100 | 4 | 6 | 2 | 1 | 13 | No | All | PSM | HES | -Unidirectional power flow |
| | [50] | 3 | 1 | 50 | 20 | 0 | 14 | 2 | 0 | 16 | No | No | DPS | DC microgrid | -High number of switches |

Note: In this table, parameters D, S, C, I, and T represent the number of diodes, switches, capacitors, inductors, and total count of components.

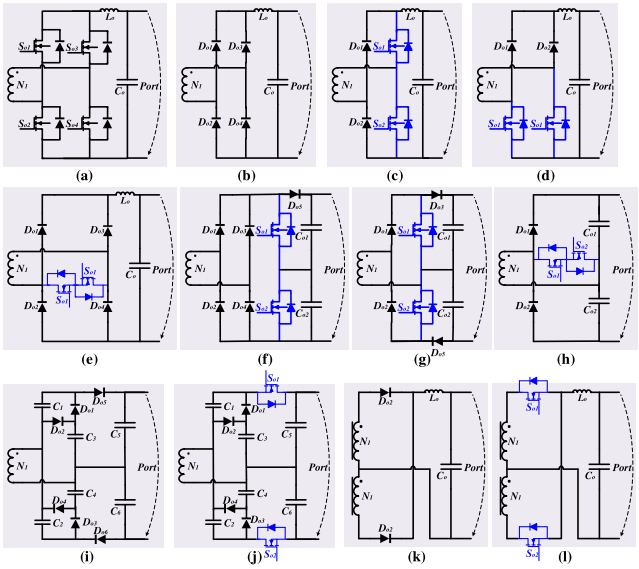

**FIGURE 12.** Different types of rectifiers for IMPCs.

**TABLE 3.** Summary of rectifier in Fig. 12.

| Circuit Fig. 13 | No. of Components | | | | | Bidirectional Capability | Current stress of semiconductors | Output Voltage Gain |
|---|---|---|---|---|---|---|---|---|
| | D | S | C | I | T | | | |
| (a) | 0 | 4 | 1 | 1 | 6 | Yes | Moderate | Medium |
| (b) | 4 | 0 | 1 | 1 | 6 | No | Moderate | Medium |
| (c) | 2 | 2 | 1 | 1 | 6 | No | Moderate | Medium |
| (d) | 2 | 2 | 1 | 1 | 6 | No | Moderate | Medium |
| (e) | 4 | 2 | 1 | 1 | 8 | No | Moderate | Medium |
| (f) | 5 | 2 | 2 | 0 | 9 | No | Low | Medium |
| (g) | 4 | 2 | 2 | 0 | 8 | No | Moderate | Medium |
| (h) | 2 | 2 | 2 | 0 | 6 | No | Moderate | Medium |
| (i) | 6 | 0 | 6 | 0 | 12 | No | High | High |
| (j) | 4 | 2 | 6 | 0 | 12 | No | High | High |
| (k) | 2 | 0 | 1 | 1 | 4 | No | High | Low |
| (l) | 0 | 2 | 1 | 1 | 4 | Yes | High | Low |

wind-solar hybrid generation system. Reference [53] presents a three-port bidirectional PIC designed for the simultaneous power management of multiple energy sources by using only three switches. It incorporates an LCL resonant circuit to enable soft-switching for the primary switch. This converter effectively interfaces sources with varying voltage-current characteristics to supply power to a load or a DC microgrid. A similar topology is proposed in [54], a three-port bidirectional PIC by combining a boost–flyback, forward converter, and voltage doubler with three switches on the secondary side of the transformer.

A three-switch converter featuring three ports is presented in [55] (Fig. 13(c)). This design incorporates two boost circuits that utilize a mutual active clamp, forming the primary input port, and a bidirectional battery port for the converter. It enables both inputs to be current-fed with a high voltage gain, making the converter particularly well-suited for RESs. In [56], a new three-port high step-up converter using a dual-charge-pump cell is proposed, which maintains a high step-up functionality without relying on extreme duty ratios or turns ratios. This design ensures continuous operation, even if one of the input sources is interrupted, but the converter does not employ soft-switching for switches (Fig. 13(d)). The topology in [40] is based on a forward converter with simplified control and fewer magnetic components (Fig. 13(a)), but it does not achieve soft switching and is limited by the maximum duty cycle due to demagnetization of the magnetic inductance. Table 4 compares these papers from different point of views. High switching loss is a major drawback observed in converters in [51], [52], and [56], primarily due to their hard-switching operations. The loss not only reduces efficiency, especially under high frequency or high power conditions, but also increases thermal stress on components, which can lead to demanding larger heatsinks or cooling systems. High volume can be considered as a limitation of converters in [53] and [55], often resulting from the use of multiple magnetics or large passive components required, which can effectively reduce their integration in compact systems. The proposed converters in [40] and [53] can provide a unidirectional power flow from the sources to the grid. This can limit the applicability of these converters in hybrid energy systems. The unclamped voltage spikes on switching devices are a major problem in [54] because of the unrecovered leakage energy in the coupled inductor. This issue could reduce the reliability and cost of the converter since switches with a higher voltage range are needed unless snubber or clamp circuits are added. The highest voltage gain is achieved by the converter [54]. This quadratic dependency on duty cycle makes it particularly suitable for applications requiring very high step-up conversion. On the other hand, the lowest voltage gain is offered by the converter in [52]. The converter in [56] provides a higher degree of freedom in the voltage gain design by adding the turn ratio of the third port to the voltage gain relation.

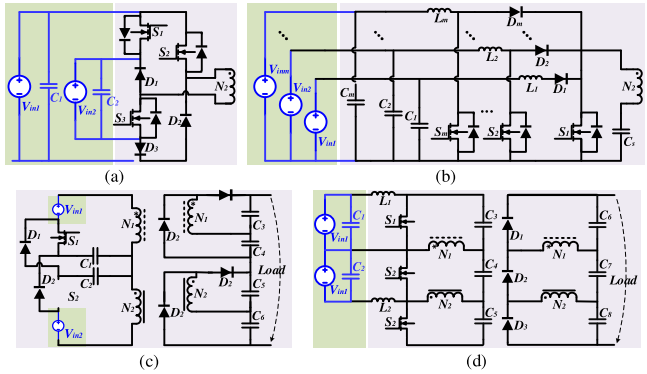

**FIGURE 13.** Other PIC topology: (a) [40], (b) [52], (c) [55], (d) [56].

In [54], soft-switching is maintained for the main switches via an LCL-based resonance circuit and appropriate gate signal timing. The effectiveness of this approach depends on the load current and the switching timing accuracy. The converter in [55] employs a snubber-free ZVS technique for all switches by forming a resonance current through the magnetizing

**TABLE 4. Summary of other PICs.**

| Other PICs | No. of Inputs | No. of Outputs | Power (W) | Frequency (kHz) | No. of Semiconductors | | | | | ZCS | ZVS | Voltage Gain | Target Applications | Disadvantages |
|---|---|---|---|---|---|---|---|---|---|---|---|---|---|---|
| | | | | | D | S | C | I | T | | | | | |
| [51] | 2 | 1 | 250 | 50 | 3 | 2 | 1 | 1 | 7 | No | No | $D/(1-D)$ | HES | -High switching losses |
| [52] | 2 | 1 | 100 | 60 | 6 | 2 | 4 | 3 | 15 | No | No | $2D/n$ | HES | -High switching losses |
| [53] | 2 | 1 | 120 | 100 | 4 | 3 | 5 | 5 | 17 | Yes | All | $1/(1-D)$ | HES | -High volume<br>-Unidirectional power flow |
| [54] | 2 | 1 | 150 | 50 | 1 | 5 | 4 | 2+1C | 13 | Yes | No | $n/(1-D)^2$ | Battery energy storage systems (BESS) | -Unclamped voltage spikes on the switches |
| [55] | 2 | 1 | 200 | 100 | 3 | 3 | 8 | 2 | 16 | Yes | All | $n/(1-D)$ | HES | -High volume |
| [56] | 2 | 1 | 200 | 50 | 6 | 2 | 6 | 2 | 16 | No | No | $\frac{n_2+n_3}{(1-D)}$ | HES | -High switching losses |
| [40] * | 2 | - | - | - | 3 | 3 | 2 | 0 | - | Yes | All | PSM | Bipolar DC bus | -Unidirectional power flow |

Note: In this table, parameters D, S, C, I, T repent the number of diodes, switches, capacitors, inductors, and total number of components. Also, in [40] only the primary side of the transformer is introduced.

inductance and parasitic capacitances across the switches. The converter in [56] combines the phase-shift modulation with calculated current paths to enable ZVS across a wide load range. To extend the soft-switching range, the optimization of resonant component sizing, phase shift tuning, and duty ratio coordination can be considered.

## III. FULLY ISOLATED CONVERTERS

FICs have a complete galvanic isolation between input and output circuits (Fig. 14), constructed with multi-winding transformers or multi-two-winding transformers to ensure isolation between each port. Their primary advantages are safety and noise immunity, essential for applications such as medical devices and electric vehicles. The separate transformer windings for each port enable easy voltage increase or decrease. However, compared to non-isolated converters, FICs have increased complexity and higher manufacturing expenses; compared to PICs, FICs ensure superior noise immunity and manage ground potential differences, but with higher complexity and cost.

Similar to PICs, FICs have two main types: half-bridge [57], [58], [59], [60], [61], [62], [63] and full-bridge [64], [65], [66], [67], [68], [69], [70], [71], [72], [73], [74], [75], [76], [77], [78], [79], [80], [81], [82], [83] (Fig. 2). Each has its own unique features that affect the performance and complexity in different FIC setups.

### A. HALF-BRIDGE-BASED FICS

The HBC features simplicity with a lower count of devices, fewer gate drivers and auxiliary power supplies, and thus, lower costs. It is efficient in managing varying input voltages, suitable for ultra-capacitors, where voltage fluctuations are prevalent.

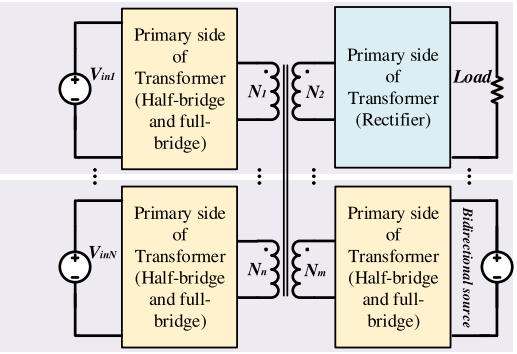


**FIGURE 14. Main architectures for FICs with three ports.**

In HBB-FICs, different circuits can be utilized for each port based on the characteristics of sources and the load. For example, using the half-bridge in Fig. 4(a) for input sources and a rectifier for the output side, three-port FICs are configured in Fig. 15(a) [57], [58]. In [57], a three-leg converter (TLC) is proposed on the secondary side of the two HFTs to minimize the circulating power between inputs. This TLC functions as an active FBC with ZVS across an extended output range, and significantly improves the overall efficiency. An LLC series resonant converter (SRC) is developed in [58] (Fig. 15(b)) using the Solid-State Transformer (SST) technology to enable DC-transformation. Power flow is divided into main and circulating power for active ports, showing the impact of the resonant tank design. Adjusting voltage differences between ports could change power distribution, affect circulating power and zero-voltage switching conditions. HBC and FBC can be combined in one topology [59], including a series-resonance-based half-bridge for

integrating ESSs, two full-bridges, and a three-winding HFT. The series-resonant network in the half-bridge minimizes the power coupling among the three ports. An integrated autonomous control method with the minimum value competition logic can effectively coordinate PV systems and ESS operations, and ensure the voltage regulation across the common bus in DC microgrids.

Another type of HBB-FIC is to use a boost HBC (Fig. 15(c)) [60], [61], [62], [63], sharing a common setup but with significantly different control strategies for switches. Reference [60] involves a triple HBC and a multi-winding transformer, which enables bidirectional power flow by adjusting phase-shift angles. Although this design allows bidirectional power flow, and the boost inductor reduces the port current ripples, but the system cost, size and bandwidth limitations are increased. An asymmetrical duty cycle control strategy implemented in a bidirectional converter in [61] manages power flow and achieves a wide ZVS range for ports interfacing with a low-voltage battery and an ultracapacitor in a FC vehicle. A triple HBC with a boost half-bridge compensates voltage variations by adjusting duty cycles [62], extends the ZVS range, and reduces the power switch stress and losses. Reference [63] reports a transformer-coupled triple-HBC, particularly beneficial for FC systems with supercapacitors or batteries, where the boost half-bridge accommodates a wide range of operation voltages, extends the ZVS operating range across the phase shift region, and reduces the current stress and switch conduction losses. These varied designs pursue efficient bidirectional power flow, reduced losses, and enhanced ZVS capabilities across diverse voltage ranges, catering to distinct energy storage in various applications. Table 5 compares HBB-FICs regarding the number of passive and active components, the rated power, etc. The converters introduced in [57], [60], and [61] suffer from a complex control method. In [57], this stems from a high number of switches, which increases the gate coordination complexity. In [60], the complexity arises from the need to achieve independent power flow and soft-switching, which requires precise timing and phase-shift control. In [61], the complexity is due to the dual control inputs (duty cycle and phase shift) per port, which must be carefully coordinated. The converters in [62] and [63] suffer from non-continuous input current at the fuel cell port, which impacts the fuel cell's lifespan and performance. The targeted application of the converter in [58] is solid-state transformers (SSTs), while its unidirectional power flow might limit its applicability where the power needs to flow in both directions.

In [57], a full ZVS is achieved across all ports by using the transformer leakage energy to discharge the parasitic capacitors across switches during the dead-time. However, a high number of switches increases control complexity. Similarly, [60] requires accurate timing and phase shift tuning to achieve ZVS under wide load and input voltage conditions. In [61], asymmetrical duty cycle control and dual control inputs, comprising duty cycle and phase shift, enable ZVS by adaptively adjusting the current slopes on each leg, which improves the soft-switching range even under variable input voltages. However, this comes at the cost of increased computational burden. The topologies introduced in [62] and [63] maintain ZVS over the full phase-shift range by using equal-duty cycle PWM across all bridges and appropriate designing of the transformer. Large input current ripples at the super capacitor port in [62] guarantee the ZVS operation although under unequal duty cycles.

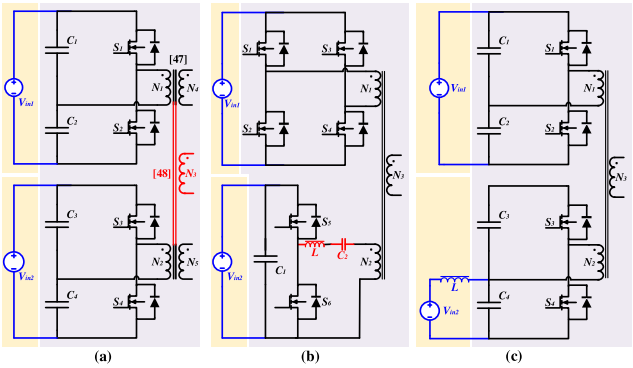


**FIGURE 15.** Different topologies for FICs, based on half-bridge. (a) [57], [58]. (b) [59]. (c) [60], [61], [62], [63].

### B. FULL-BRIDGE-BASED FICS

While HBB features simplicity and can handle different input voltages, FBB provides higher power, better stress sharing across the switches, and bidirectional power flow for applications requiring reversible power transfer, such as electric vehicles (EVs) or the regenerative braking operation of ESSs. However, FBB has the increased complexity, a higher number of components, and a higher cost.

The first category of FBB-FICs is the extension of the DAB topology, a three-port triple-active-bridge (TAB) converter and a four-port quad-active-bridge (QAB) converter. In [64], [65], [66], [67], [68], [69], [70], [71], [72], [73], [74], and [75], different types of TABs and QABs are introduced. DAB converters offer the reduced device stress, bidirectional power flow, fixed-frequency operation, and energy transfer using transformer leakage inductance. TAB converters are widely used in RESs, UPSs, and EVs, featured by simplicity, soft switching, especially suitable for applications requiring a high power density, quick response, and the bidirectional power flow. However, they cannot handle a broad input voltage range, such as with FCs and super-capacitors. When the input voltages differ across three ports, a significant increase in circulating current may occur, and the converter may lose its soft switching ability when there are fluctuations in input voltages and the load. TAB converters also face a DC bias issue that could cause saturation of the transformer core. In [64], [65], [66], [67], [68], [69], and [70], the same TAB circuit in Fig. 16(a) uses different modulation and control techniques to achieve ZVS, which minimizes switching losses and manages electromagnetic interference (EMI). TABs are symmetrical and isolated from each other.

**TABLE 5. Summary of HBB-FICs.**

| HBB-FICs | No. of Inputs | No. of Outputs | Power (W) | Frequency (kHz) | No. of Components | | | | | ZCS | ZVS | Voltage Gain | Target Applications | Disadvantages |
|---|---|---|---|---|---|---|---|---|---|---|---|---|---|---|
| | | | | | D | S | C | I | T | | | | | |
| [57] | 2 | 1 | 1000 | 20 | 0 | 10 | 5 | 0 | 15 | No | All | $1/(1-2D)$ | HES | -Complex control method |
| [58] | 2 | 1 | 4000 | 12 | 2 | 4 | 8 | 2 | 16 | Yes | All | Not mentioned | SST | -Unidirectional power flow |
| [59] | 2 | 1 | 1000 | 40 | 0 | 10 | 4 | 3 | 17 | No | All | PSM | DC microgrid | -High volume |
| [60] | 2 | 1 | 6000 | 20 | 0 | 6 | 7 | 2 | 15 | No | All | PSM | HES | -Complex control method |
| [61] | 2 | 1 | 2000 | 20 | 0 | 6 | 7 | 2 | 15 | No | All | PSM | Fuel cell vehicles | -Complex control method |
| [62] | 2 | 1 | 1000 | 20 | 0 | 6 | 8 | 1 | 15 | No | All | $1/D$ | Fuel cell | -Non-continuous input current at the fuel cell port |
| [63] | 2 | 1 | 2000 | 20 | 0 | 6 | 8 | 1 | 15 | No | All | $1/D$ | Fuel cell | -Non-continuous input current at the fuel cell port |

Note: In this table, parameters D, S, C, and I represent the number of diodes, switches, capacitors, and inductors.

Reference [64] introduces a technique involving the duty ratio and phase shift control to expand the ZVS operational range by using a pre-calculated lookup table based on the output current and voltage (the V-I plane) as parameters to control the delay angle of firing signals of one bridge leg, ensuring soft-switching across all switches. Besides the phase shift control to manage power flow between the ports, utilization of the duty cycle control to optimize the system behavior is discussed in [65]. Optimization techniques, such as minimizing the overall system losses and ensuring zero circulating currents within the converter, contribute to the efficient power conversion, reduced weight, and compact construction. Reference [66] focuses on ZVS for switches across a broad input voltage spectrum, but shows challenges due to significant EMI, limitations in size, and power losses associated with the transformer-coupled design. Reference [67] utilizes SSTs and silicon carbide (SiC) in high-power, high-efficiency TABs, achieving the reduced turn-on losses, enhanced system reliability, and increased power density due to faster switching speeds and lower losses of SiC devices compared to silicon-based converters. Their design optimization is crucial to obtain a high efficiency while managing turn-off losses, voltage oscillations, and temperature rise, particularly in SiC-based systems. The proposed TAB converter enables power transmission among its three ports by regulating phase shift angles of three H-bridge converters. An alternative SST topology based on the QAB converter is proposed in [68] by incorporating a control technique specifically custom-made for the dc-dc stage of the QAB-based SST, PVs and BSSs. The technique addresses cross-coupling features of the QAB converter to enhance the regulation of a high-voltage DC link. The ZVS region is derived in [69] and [70] by considering parameters, such as switch capacitance, transformer inductance, and operating conditions to reduce switching losses and EMI. To improve efficiency of TAB converters, conduction losses are minimized through PWM scheme optimization, multiple control variables are employed for modulation flexibility, and gradient descent algorithms are used under various operating conditions [70]. In [71], automatic voltage balancing for bipolar DC distribution for TABs is proposed by eliminating dedicated voltage-balancing controllers and extra components and using the magnetic integration of the converter's existing inductors. This integrated voltage balancing coupled inductor enables power transfer, ZVS, and voltage balancing without increasing the converter's magnetic volume, and thus, improves the converter's efficiency.

References [72] and [73] investigate innovative dual-transformer-based configurations for TAB converters, such as DT-ATAB (Fig. 16 (b)), which uses dual transformers to solve the problems, such as the magnetic short-circuit, and achieve the improved power management with reduced losses and enhanced current balancing among ports. While the control of DT-ATAB is relatively simple due to separate transformers, it still requires a higher number of switching devices and transformer cores. Various trade-offs in the converter design are essential to achieve the improved performance while overcoming drawbacks in conventional TAB converters.

An alternative setup of TAB and DT-ATAB converters adopts a buck/boost interleaved structure as a current-fed source, as shown in Fig. 16(c) [74], [75]. This configuration employs two identical parallel inductors to alleviate stress of currents on individual switches, ensuring a more consistent input current from the sources. It can manage wide fluctuations in input voltage through the duty ratio control, and thus, reduce the system stress and improve efficiency. It eliminates requirements of transformer windings and switch current ratings compared to conventional TAB

in Fig. 16(a). This topology can be combined with series resonant cells. By aligning the switching frequency with the resonant frequency of the high-voltage resonant tank, power decoupling is accomplished, allowing precise control of the power transfer. This design eliminates the coupled power between low-voltage side ports, and simplifies the analysis through resonant-type energy storage loops. An optimized modulation strategy has increased its efficiency. It addresses issues in current-fed converters, achieves precise power control, reduces current stress, and has higher efficiency than voltage-fed converters.

Other types of FBB-FICs in [76], [77], and [78] are TPCs with a two-leg diode rectifier as their load at the output. Reference [76] proposes a flux additivity-based converter, which can draw power from two different DC sources and deliver power simultaneously to the load, but reverse-blocking diodes lead to unidirectional power flow, which restricts its use for energy storage. Reference [77] proposes a topology employing auxiliary switches to ensure zero circulating current between ports, while allowing bidirectional power flow; it offers a simpler switching scheme and avoids the need of external inductors in conventional topologies, such as the TAB. An isolated high-frequency converter for PV systems with a two-quadrant inverter topology is proposed in [78] to prevent circulating currents between ports, and ensure efficient power transfer from each PV module without the current flow from AC to DC sides.

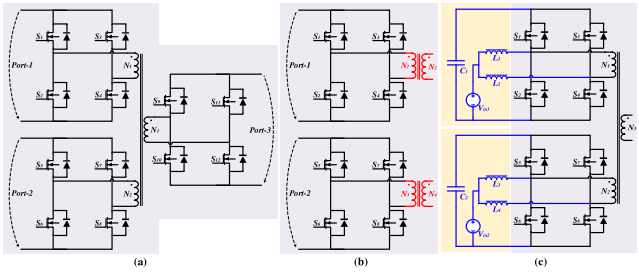


**FIGURE 16.** Different topologies for FICs, based on full-bridge: (a) [64], [65], [66], [67], [68], [69], [70]. (b) [72], [73]. (c) [74], [75].

Three-port resonant converters are introduced in [79], [80], [81], [82], and [83]. Resonant converters are appealing for RESs due to their ZVS capabilities and high-frequency operation. A single high-frequency transformer UPS is introduced in [79] for galvanic isolation for load and battery with a high input power factor and trapezoidal output voltage waveforms at varying frequencies, and a LC filter is used at the input of the line-side converter (LSC). This filter eliminates high-frequency current components and offers a pathway for the currents originating from the LSC. The parallel resonant capacitor aims to reduce voltage stresses on the output diode rectifier while supplying necessary amplification for stable operation at a constant output DC bus voltage and a high input power factor. In contrast, [80] focuses on a bidirectional multi-element resonant converter employing various resonant frequencies strategically positioned to transfer active power efficiently. The multi-element resonant tank comprises three resonant frequencies in total: two series resonant frequencies and one notch resonant frequency. Reference [81] proposes a TPC utilizing active full bridges and two series resonant tanks to control power flow between batteries, RESs, and the load. A control strategy is proposed to minimize power coupling by elevating the ratio between the resonant and switching frequencies as a higher ratio reduces the power coupling while maintaining the same power transfer. Nevertheless, this modulation strategy cannot achieve the complete power decoupling. Reference [82] innovatively combines 380 V and 48 V dc power distributions via a three-port LCC resonant converter, and reduces power conversion steps and losses. The LCC resonant tank helps to achieve ZVS for all switches and ZCS for rectifying diodes, aided by a single-capacitor filter. A two-degree-of-freedom control that merges phase shift and frequency variation is used to achieve soft switching and a high efficiency. Reference [83] presents an TPC with series resonant and DABs for EV charging stations, this design has a simple control, and the reduced system cost and volume. Although resonant converters offer advantages, such as ZVS and reduced EMI, managing power flow between ports remains challenging, and necessitates intricate control algorithms for power decoupling. Table 6 compares the FBB-FIC topologies and categorizes them. Based on this table, [68] presents a converter suitable for SST applications, but the highest number of switches is used, making its control circuit complex. The resonant converters in [80], [81], [82], and [83] apply a variable frequency modulation (VFM) to achieve ZVS across all switches and enhance efficiency. The unidirectional port in [83] limits its application in future bidirectional charging scenarios. The converters in [72] and [79] utilize a magnetic core to provide isolation between ports and provide ZVS. These benefits come at the cost of a higher volume of the converter. Reference [67] tries to reduce the volume of the converter using the wide-band-gap devices, but the ZVS operation of the converter is sensitive to parasitic elements, such as switches and inductor's resistors.

## IV. FUTURE TRENDS

With increasing integration of RESs and BSSs in power grids, and the rise of zero-carbon transportation like electric and hybrid vehicles, the demand for efficient MPCs is growing. The future of IMPCs depends on technical advances that enhance the efficiency, reliability, resiliency, and sustainability of power conversion solutions. Fig. 17 presents a comparative analysis of different categories of IMPCs in terms of qualitative performance metrics and quantitative hardware complexity. In Fig. 17(a), the spiderweb chart illustrates relative performance across attributes, such as the cost, power density, power level, control simplicity, efficiency, reliability, complexity, and weight. Each attribute is rated on a normalized scale from 0 to 10, with 10 representing the most favorable performance. The ratings were derived from trends

**TABLE 6. Summary of FBB-FICs.**

| Circuit | Full-Bridge-Base FICs | No. of Inputs | No. of Outputs | Power (W) | Frequency (kHz) | No. of Components | | | | | ZCS | ZVS | Control method | Target Applications | Disadvantages |
|---|---|---|---|---|---|---|---|---|---|---|---|---|---|---|---|
| | | | | | | D | S | C | I | T | | | | | |
| TAB | [64] | 2 | 1 | 500 | 100 | 0 | 12 | 3 | 0 | 15 | No | No | PSM | Fuel cell | -High switching losses |
| | [65] | 2 | 1 | 1500 | 100 | 0 | 12 | 1 | 0 | 13 | No | No | PSM | HES | -High switching losses |
| | [66] | 2 | 1 | 1000 | 20 | 0 | 12 | 3 | 0 | 15 | Yes | All | PSM | HES | -Requires active duty-ratio control per port |
| | [67] | 2 | 1 | 150 | 50 | 0 | 12 | 1 | 0 | 13 | Yes | All | PSM | HES | -Sensitivity to the parasitic elements |
| | [68] | 3 | 1 | 960 | 20 | 0 | 16 | 4 | 0 | 20 | No | All | PSM | SST | -Complex control circuit |
| | [69] | 2 | 1 | - | 50 | 0 | 12 | 3 | 0 | 15 | No | All | PSM | HES | -Under light load, the ZVS is not guaranteed for the lower voltage ports |
| | [70] | 2 | 1 | 600 | 100 | 0 | 12 | 2 | 0 | 14 | No | All | DPS | HES | -Computational burden due to optimal multi-variable control |
| | [71] | 1 | 2 | 5000 | 20 | 0 | 12 | 3 | 2C | 17 | No | All | DPS | Bipolar DC bus | -Leakage inductance directly affects the output voltages. |
| DT-ATAB | [72] | 2 | 1 | 1000 | 20 | 0 | 14 | 1 | 0 | 15 | No | All | PSM | HES | -Two separate transformers are needed |
| | [73] | 2 | 1 | 600 | 15 | 0 | 14 | 1 | 0 | 15 | No | All | DPS | DC microgrid | -Complex control circuit |
| Interleaved TAB | [74] | 2 | 1 | 1000 | 25 | 0 | 12 | 3 | 4 | 19 | No | No | PSM | Fuel cell | -High switching losses |
| | [75] | 2 | 1 | 600 | 50 | 0 | 12 | 6 | 4 | 22 | No | All | PSM | HES | -High volume |
| Three-Port Converters | [76] | 2 | 1 | 200 | 50 | 4 | 8 | 0 | 1 | 13 | No | No | PSM | HES | -High switching losses |
| | [77] | 2 | 1 | 300 | 10 | 4 | 8 | 3 | 1 | 16 | No | Not All | Not mentioned | HES | -High switching losses |
| | [78] | 2 | 1 | 500 | 10 | 4 | 8 | 3 | 1 | 16 | Yes | No | Not mentioned | DC microgrid | -High switching losses |
| Resonant Converters | [79] | 2 | 1 | 500 | 100 | 4 | 8 | 6 | 1 | 19 | No | All | VFM | HFC | -Auxiliary inductor added solely to keep ZVS at low battery current |
| | [80] | 2 | 1 | 750 | 95 | 0 | 12 | 7 | 2 | 21 | No | All | VFM | HES | -High volume |
| | [81] | 2 | 1 | 500 | 100 | 0 | 12 | 5 | 2 | 19 | No | All | VFM | HES | -The input voltages need to be higher than the output voltage for ZVS. |
| | [82] | 2 | 1 | 600 | 240-320 | 4 | 8 | 6 | 2 | 20 | Yes | All | VFM | DC microgrid | -High volume |
| | [83] | 1 | 2 | 5000 | 150 | 4 | 8 | 4 | 2 | 18 | Yes | All | VFM | EVs | -Unidirectional power flow at the fast charging port |

Note: In this table, parameters D, S, C, I, and T represent the number of diodes, switches, capacitors, inductors, and total count of components.

consistently observed in the literature, supported by data, such as power ratings, efficiency benchmarks, and component counts, discussed in this work. In Fig. 17(b), the bar chart compares the normalized number of components, such as diodes, switches, capacitors, inductors, and transformers, that are used in typical implementations of each IMPC category. Raw component values were obtained from representative topologies and normalized to a common base (HBB-PICs) for consistency. Table 7 reviewed advantages, disadvantages, and typical applications of PICs and FICs.

### A. COMPACT HIGH-EFFICIENCY IMPCS

High power density and efficiency are highly desirable, especially for electric and hybrid vehicles, in which volume and mass are very critical. Improving power density and efficiency can significantly lower initial investment and operation costs through a reduced component count, size, and power losses. To improve power density and efficiency of IMPCs, new transformer technologies, such as HFTs and SSTs, can replace traditional bulky LFTs. HFTs offer higher power density and efficiency as they operate

at higher frequencies, allowing smaller core sizes and less losses [23], [25], [48], [57]. SSTs have higher power density and efficiency with greater control and flexibility via power electronics, are compact and reliable, but more costly and complicated to implement [58], [67], [68].

Wide-bandgap (WBG) devices, such as SiC and GaN, have a broader energy bandgap than conventional silicon-based devices, can operate at higher temperatures and voltages, suitable for high power and high frequency applications. WBG devices also have lower resistance and faster switching speeds, which further decreases conduction and switching losses, and increases the overall efficiency and power density [87], [88]. However, WBG devices have lower parasitic capacitance that increases the vulnerability of EMI [89]. The proper circuit board design is thus necessary to reduce parasitical parameters and ensure reliability. Developing compact, high efficiency IMPCs using WBG devices is a promising future research area.

### B. BIDIRECTIONAL OPERATION OF IMPCS

Bidirectional IMPCs are essential for ESSs in RESs integration. Bidirectional feature is easier to achieve in isolated converters than in non-isolated converters. This feature reduces the overall system size and cost, but requires complex control. The future research should focus on optimizing control strategies of bidirectional IMPCs.

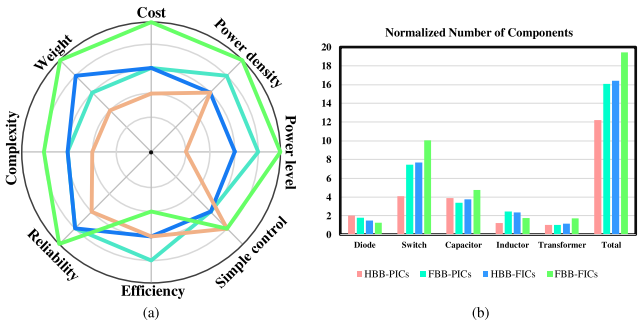


**FIGURE 17.** IMPCs: (a) Comparative analysis, (b) Normalized number of components.

### C. RELIABILITY AND RESILIENCY OF IMPCS

Resiliency is a critical feature in power converter design, especially in applications demanding high availability, such as remote renewable energy systems, electric vehicle chargers, and communication infrastructure. Resiliency refers to the system's ability to withstand, adapt to, and recover from internal faults or external disturbances while maintaining continued operation and minimal service disruption [93]. Since power converters are among the most failure-prone elements in power electronic systems, primarily due to semiconductor device failures [91], their design must explicitly incorporate strategies to improve fault tolerance and system robustness.

Reliability-oriented design begins with minimizing the failure rate through derating, thermal management, and reducing electrical stress. Design considerations, such as lower current and voltage stress, optimized switching patterns, efficient thermal dissipation, and reduced conduction and switching losses help extend the converter's lifespan and operating reliability [90]. However, due to device aging, environmental stress, and unforeseen conditions, such as grid fluctuations or EMI, complete fault avoidance is impractical. Hence, resiliency methods are necessary to maintain the system's functionality during fault events.

Resiliency techniques can be broadly classified into redundant hardware-based approaches and control-based fault tolerance schemes [94], [95], [96], [97]. Redundant approaches provide additional hardware, such as extra switches or power paths, to maintain power delivery in the presence of faults. For example, [101] proposes a fault-resilient H-bridge converter equipped with 28 additional semiconductor switches to tolerate all types of switch faults while fully satisfying load demands. Although such methods ensure high resilience, they impose substantial penalties in terms of the cost, volume, and control complexity due to the required sensors, gate drivers, and monitoring systems. Control-based techniques, on the other hand, modify the modulation or control logic to accommodate faults using the same hardware, which are more cost-effective but typically maintain operation at reduced power levels. A control-based method is introduced in [102], where open-circuit and short-circuit faults are detected by comparing the measured inductor current to the predicted reference values. This method relies only on measurements under normal operation, localizes faults quickly, and requires

**TABLE 7.** Comparison of IMPCs.

| Group | Advantages | Disadvantages | Applications |
|---|---|---|---|
| HBB-PICs | - Simple design<br>- Simple control strategies<br>- Lower component count<br>- Reduced cost and size | - Limited power handling capabilities<br>- Higher transformer losses | - RESs (low to moderate)<br>- BSSs<br>- Residential energy storage<br>- Portable electronic devices |
| FBB-PICs | - Reduced voltage stress across switches<br>- Higher efficiency<br>- Better output voltage quality and reduced ripples<br>- Higher power converter | - Higher component count<br>- Higher cost and complexity<br>- Larger and heavier compared to HBB | - RESs (High)<br>- Industrial power supplies<br>- EVs<br>- Industrial UPS systems |
| HBB-FICs | - Complete galvanic isolation<br>- Higher safety and noise immunity<br>- Easy voltage increase or decrease via separate transformer windings | - Increased complexity<br>- Higher manufacturing costs<br>- Higher transformer losses | - Medical devices<br>- High-voltage BSSs<br>- Telecom power systems<br>- Sensitive instrumentation systems |
| FBB-FICs | - Complete galvanic isolation<br>- Higher safety and noise immunity<br>- Suitable for high-power applications requiring full isolation<br>- Bidirectional capability | - Increased complexity<br>- Higher manufacturing costs<br>- Larger and heavier compared to HBB | - Aerospace and defense systems<br>- High-power industrial motor drives<br>- High-performance EVs |

no extra hardware. However, it cannot fully meet load demand during faults and is better suited for non-isolated converters.

For full-bridge converters, a widely adopted method is to allow the converter to operate as a half-bridge upon a single switch failure. Although this might reduce the output voltage to half, the converter can continue supplying power. To compensate for this drop, a voltage doubler circuit can be added [98], [99], in which an auxiliary switch remains off during normal operation and turns on when a fault is detected. This method can effectively restore the output voltage to its nominal level, and enhance resilience with a minimal additional cost.

In dual-active bridge converters, a more advanced technique known as triple-phase shift (TPS) modulation is proposed to increase the fault tolerance [100]. TPS allows diagnosis of fault type and location by monitoring the midpoint voltage of converter legs. Once the fault is detected, only the faulty leg is deactivated, and a new phase shift is applied to maintain the operation of the converter. Therefore, the converter continues to supply the load at a reduced output level. This control-based method achieves both resilience and reliability without significant circuit modification.

Lastly, design optimizations in the resonant structure can contribute to resiliency by ensuring ZVS/ZCS operation over wide load ranges, reducing thermal stress, and extending device life-time. However, under light-load or very high switching frequency, even resonant converters may face challenges maintaining soft-switching, which could increase the risk of faults.

In conclusion, effective resiliency design in power converters is a multi-faceted challenge involving a trade-off between the cost, complexity, and fault coverage. Future research should aim to develop hybrid methods that combine a minimal redundancy with intelligent control, offering resilience without excessive overhead. Moreover, machine-learning-based diagnostics and reconfigurable control architectures may hold promise in enhancing fault prediction and real-time adaptability.

## V. CONCLUSION

This paper provides a comprehensive literature review for isolated multi-port DC-DC converters for various energy sources and storage systems integration. This review highlights advantages and challenges of partially isolated converters and fully isolated converters, and covers essential design criteria, including soft switching, bidirectional capability, voltage gains, component review, and resiliency techniques for IMPCs. The future research directions are recommended for IMPCs, considering advances in semiconductors and transformer technologies.

## REFERENCES


[1] A. Affam, Y. M. Buswig, A.-K.-B. H. Othman, N. B. Julai, and O. Qays, "A review of multiple input DC–DC converter topologies linked with hybrid electric vehicles and renewable energy systems," *Renew. Sustain. Energy Rev.*, vol. 135, Jan. 2021, Art. no. 110186.

[2] A. Asadi, M. S. Karimzadeh, X. Liang, M. S. Mahdavi, and G. B. Gharehpetian, "A novel control approach for a single-inductor multi-input single-output DC–DC boost converter for PV applications," *IEEE Access*, vol. 11, pp. 114753–114764, 2023.

[3] G. Chen, Y. Liu, X. Qing, M. Ma, and Z. Lin, "Principle and topology derivation of single-inductor multi-input multi-output DC–DC converters," *IEEE Trans. Ind. Electron.*, vol. 68, no. 1, pp. 25–36, Jan. 2021.

[4] R. K. Kanaparthi, J. P. Singh, and M. S. Ballal, "A review on multi-port bidirectional isolated and non-isolated DC–DC converters for renewable applications," in *Proc. IEEE Int. Conf. Power Electron., Drives Energy Syst. (PEDES)*, Dec. 2022, pp. 1–6.

[5] E. Amiri, R. R. Khorasani, E. Adib, and A. Khoshkbar-Sadigh, "Multi-input high step-up DC–DC converter with independent control of voltage and power for hybrid renewable energy systems," *IEEE Trans. Ind. Electron.*, vol. 68, no. 12, pp. 12079–12087, Dec. 2021.

[6] R. Liu, G. Zhou, Q. Tian, and G. Xu, "Extendable multiport high step-up DC–DC converter for photovoltaic-battery systems with reduced voltage stress on switches/diodes," *IEEE Trans. Ind. Electron.*, vol. 70, no. 9, pp. 9123–9135, Sep. 2023.

[7] A. Shoaei, K. Abbaszadeh, and H. Allahyari, "A single-inductor multi-input multilevel high step-up DC–DC converter based on switched-diode-capacitor cells for PV applications," *IEEE J. Emerg. Sel. Topics Ind. Electron.*, vol. 4, no. 1, pp. 18–27, Jan. 2023.

[8] N. Gaurav, N. Jayaram, S. Halder, K. P. Panda, and S. V. K. Pulavarthi, "A novel design with condensed component of multi-input high gain nonisolated DC–DC converter for performance enhancement in carbon neutral energy application," *IEEE J. Emerg. Sel. Topics Ind. Electron.*, vol. 4, no. 1, pp. 37–49, Jan. 2023.

[9] S. M. Taheri, A. Baghramian, and S. A. Pourseyedi, "A novel high-step-up SEPIC-based nonisolated three-port DC–DC converter proper for renewable energy applications," *IEEE Trans. Ind. Electron.*, vol. 70, no. 10, pp. 10114–10122, Oct. 2023.

[10] O. Balapanuru, M. M. Lokhande, and M. Aware, "Nonisolated integrated boost featured (NIIBF) multi-input ultrahigh gain DC–DC converter," *IEEE Trans. Power Electron.*, vol. 39, no. 5, pp. 5682–5694, May 2024.

[11] A. Asadi, K. Abbaszadeh, and A. Darabi, "Modeling and control of a single-inductor multi-input multi-output DC–DC boost converter for PV applications," in *Proc. 13th Power Electron., Drive Syst., Technol. Conf. (PEDSTC)*, Feb. 2022, pp. 51–55.

[12] G.-J. Su and F. Z. Peng, "A low cost, triple-voltage bus DC–DC converter for automotive applications," in *Proc. 20th Annu. IEEE Appl. Power Electron. Conf. Expo.*, vol. 2, Jul. 2005, pp. 1015–1021.

[13] G.-J. Su and L. Tang, "A reduced-part, triple-voltage DC–DC converter for EV/HEV power management," *IEEE Trans. Power Electron.*, vol. 24, no. 10, pp. 2406–2410, Oct. 2009.

[14] H. Wu, R. Chen, J. Zhang, Y. Xing, H. Hu, and H. Ge, "A family of three-port half-bridge converters for a stand-alone renewable power system," *IEEE Trans. Power Electron.*, vol. 26, no. 9, pp. 2697–2706, Sep. 2011.

[15] H. Al-Atrash, F. Tian, and I. Batarseh, "Tri-modal half-bridge converter topology for three-port interface," *IEEE Trans. Power Electron.*, vol. 22, no. 1, pp. 341–345, Jan. 2007.

[16] Z. Qian, O. Abdel-Rahman, H. Al-Atrash, and I. Batarseh, "Modeling and control of three-port DC/DC converter interface for satellite applications," *IEEE Trans. Power Electron.*, vol. 25, no. 3, pp. 637–649, Mar. 2010.

[17] Z. Qian, O. Abdel-Rahman, and I. Batarseh, "An integrated four-port DC/DC converter for renewable energy applications," *IEEE Trans. Power Electron.*, vol. 25, no. 7, pp. 1877–1887, Jul. 2010.

[18] J. Zeng, J. Ning, X. Du, T. Kim, Z. Yang, and V. Winstead, "A four-port DC–DC converter for a standalone wind and solar energy system," *IEEE Trans. Ind. Appl.*, vol. 56, no. 1, pp. 446–454, Jan. 2020.

[19] H. Wu, K. Sun, L. Zhu, and Y. Xing, "An interleaved half-bridge three-port converter with enhanced power transfer capability using three-leg rectifier for renewable energy applications," *IEEE J. Emerg. Sel. Topics Power Electron.*, vol. 4, no. 2, pp. 606–616, Jun. 2016.

[20] Z. Saadatizadeh, P. C. Heris, and A. Mantooth, "High-frequency three-port DC–DC converter with zero-voltage switching operation," *IEEE Trans. Ind. Electron.*, vol. 71, no. 1, pp. 537–548, Jan. 2024.

[21] H. Zhu, D. Zhang, H. S. Athab, B. Wu, and Y. Gu, "PV isolated three-port converter and energy-balancing control method for PV-battery power supply applications," *IEEE Trans. Ind. Electron.*, vol. 62, no. 6, pp. 3595–3606, Jun. 2015.

[22] H. Tao, A. Kotsopoulos, J. L. Duarte, and M. A. M. Hendrix, "Multi-input bidirectional DC–DC converter combining DC-link and magnetic-coupling for fuel cell systems," in *Proc. 40th IAS Annu. Meeting. Conf. Rec. Ind. Appl. Conf.*, vol. 3, Oct. 2005, pp. 2021–2028.

[23] M. M. Savrun and A. Atay, "Multiport bidirectional DC–DC converter for PV powered electric vehicle equipped with battery and supercapacitor," *IET Power Electron.*, vol. 13, no. 17, pp. 3931–3939, Dec. 2020.

[24] P. Kolahian, H. Tarzamni, A. Nikafrooz, and M. Hamzeh, "Multi-port DC–DC converter for bipolar medium voltage DC micro-grid applications," *IET Power Electron.*, vol. 12, no. 7, pp. 1841–1849, Jun. 2019.

[25] J. Hong, J. Yin, Y. Liu, J. Peng, and H. Jiang, "Energy management and control strategy of photovoltaic/battery hybrid distributed power generation systems with an integrated three-port power converter," *IEEE Access*, vol. 7, pp. 82838–82847, 2019.

[26] H. Wu, P. Xu, H. Hu, Z. Zhou, and Y. Xing, "Multiport converters based on integration of full-bridge and bidirectional DC–DC topologies for renewable generation systems," *IEEE Trans. Ind. Electron.*, vol. 61, no. 2, pp. 856–869, Feb. 2014.

[27] H. Wu, J. Zhang, X. Qin, T. Mu, and Y. Xing, "Secondary-Side-Regulated soft-switching full-bridge three-port converter based on bridgeless boost rectifier and bidirectional converter for multiple energy interface," *IEEE Trans. Power Electron.*, vol. 31, no. 7, pp. 4847–4860, Jul. 2016.

[28] Z. Ding, C. Yang, Z. Zhang, C. Wang, and S. Xie, "A novel soft-switching multiport bidirectional DC–DC converter for hybrid energy storage system," *IEEE Trans. Power Electron.*, vol. 29, no. 4, pp. 1595–1609, Apr. 2014.

[29] W. Li, J. Xiao, Y. Zhao, and X. He, "PWM plus phase angle shift (PPAS) control scheme for combined multiport DC/DC converters," *IEEE Trans. Power Electron.*, vol. 27, no. 3, pp. 1479–1489, Mar. 2012.

[30] A. K. Bhattacharjee and I. Batarseh, "An interleaved boost and dual active bridge-based single-stage three-port DC–DC–AC converter with sine PWM modulation," *IEEE Trans. Ind. Electron.*, vol. 68, no. 6, pp. 4790–4800, Jun. 2021.

[31] T. Chaudhury and D. Kastha, "A high gain multiport DC–DC converter for integrating energy storage devices to DC microgrid," *IEEE Trans. Power Electron.*, vol. 35, no. 10, pp. 10501–10514, Oct. 2020.

[32] S. Kurm and V. Agarwal, "Dual active bridge based reduced stage multiport DC/AC converter for PV-battery systems," *IEEE Trans. Ind. Appl.*, vol. 58, no. 2, pp. 2341–2351, Mar. 2022.

[33] Q. Tian, G. Zhou, L. Wang, Q. Bi, and M. Leng, "Symmetric bipolar output full-bridge four-port converter with phase-shift modulated Buck–Boost voltage balancer," *IEEE Trans. Ind. Electron.*, vol. 69, no. 8, pp. 8040–8054, Aug. 2022.

[34] J. Deng, H. Wang, and M. Shang, "A ZVS three-port DC/DC converter for high-voltage bus-based photovoltaic systems," *IEEE Trans. Power Electron.*, vol. 34, no. 11, pp. 10688–10699, Nov. 2019.

[35] M. C. Mira, Z. Zhang, A. Knott, and M. A. Andersen, "Analysis, design, modeling, and control of an interleaved-boost full-bridge three-port converter for hybrid renewable energy systems," *IEEE Trans. Power Electron.*, vol. 32, no. 2, pp. 1138–1155, Feb. 2017.

[36] J. Zhang, H. Wu, X. Qin, and Y. Xing, "PWM plus secondary-side phase-shift controlled soft-switching full-bridge three-port converter for renewable power systems," *IEEE Trans. Ind. Electron.*, vol. 62, no. 11, pp. 7061–7072, Nov. 2015.

[37] W. Li, C. Xu, H. Luo, Y. Hu, X. He, and C. Xia, "Decoupling-controlled triport composited DC/DC converter for multiple energy interface," *IEEE Trans. Ind. Electron.*, vol. 62, no. 7, pp. 4504–4513, Jul. 2015.

[38] J. Zeng, X. Du, and Z. Yang, "A multiport bidirectional DC–DC converter for hybrid renewable energy system integration," *IEEE Trans. Power Electron.*, vol. 36, no. 11, pp. 12281–12291, Nov. 2021.

[39] X. Sun, Y. Shen, W. Li, and H. Wu, "A PWM and PFM hybrid modulated three-port converter for a standalone PV/battery power system," *IEEE J. Emerg. Sel. Topics Power Electron.*, vol. 3, no. 4, pp. 984–1000, Dec. 2015.

[40] Q. Tian, G. Zhou, H. Li, Y. Yang, and D. Zhou, "Symmetrical bipolar output isolated four-port converters based on center-tapped winding for bipolar DC bus applications," *IEEE Trans. Power Electron.*, vol. 37, no. 2, pp. 2338–2351, Feb. 2022.

[41] D. Sha, X. Wang, K. Liu, and C. Chen, "A current-fed dual-active-bridge DC–DC converter using extended duty cycle control and magnetic-integrated inductors with optimized voltage mismatching control," *IEEE Trans. Power Electron.*, vol. 34, no. 1, pp. 462–473, Jan. 2019.

[42] P. Wang, P. Ren, X. Lu, W. Wang, and D. Xu, "Topology analysis and power sharing control of a two-stage three-port hybrid energy storage converter for DC microgrids," *IEEE J. Emerg. Sel. Topics Power Electron.*, vol. 9, no. 1, pp. 647–665, Feb. 2021.

[43] S. Kurm and V. Agarwal, "Interfacing standalone loads with renewable energy source and hybrid energy storage system using a dual active bridge based multi-port converter," *IEEE J. Emerg. Sel. Topics Power Electron.*, vol. 10, no. 4, pp. 4738–4748, Aug. 2022.

[44] H. Wu, K. Sun, R. Chen, H. Hu, and Y. Xing, "Full-bridge three-port converters with wide input voltage range for renewable power systems," *IEEE Trans. Power Electron.*, vol. 27, no. 9, pp. 3965–3974, Sep. 2012.

[45] A. Vettuparambil, K. Chatterjee, and B. G. Fernandes, "Dual-Active-Bridge-Based multiport converter with split DC links," *IEEE Trans. Ind. Electron.*, vol. 69, no. 1, pp. 485–494, Jan. 2022.

[46] A. Vettuparambil, K. Chatterjee, and B. G. Fernandes, "A multiport converter interfacing solar photovoltaic modules and energy storage with DC microgrid," *IEEE Trans. Ind. Electron.*, vol. 68, no. 4, pp. 3113–3123, Apr. 2021.

[47] H. Wu, Y. Jia, F. Yang, L. Zhu, and Y. Xing, "Two-stage isolated bidirectional DC–AC converters with three-port converters and two DC buses," *IEEE J. Emerg. Sel. Topics Power Electron.*, vol. 8, no. 4, pp. 4428–4439, Dec. 2020.

[48] K. Itoh, M. Ishigaki, N. Yanagizawa, S. Tomura, and T. Umeno, "Analysis and design of a multiport converter using a magnetic coupling inductor technique," *IEEE Trans. Ind. Appl.*, vol. 51, no. 2, pp. 1713–1721, Mar. 2015.

[49] J. Zhang, W. Jiang, T. Jiang, S. Shao, Y. Sun, B. Hu, and J. Zhang, "A three-port LLC resonant DC/DC converter," *IEEE J. Emerg. Sel. Topics Power Electron.*, vol. 7, no. 4, pp. 2513–2524, Dec. 2019.

[50] V. Karthikeyan and R. Gupta, "Multiple-input configuration of isolated bidirectional DC–DC converter for power flow control in combinational battery storage," *IEEE Trans. Ind. Informat.*, vol. 14, no. 1, pp. 2–11, Jan. 2018.

[51] N. D. Benavides and P. L. Chapman, "Power budgeting of a multiple-input buck-boost converter," *IEEE Trans. Power Electron.*, vol. 20, no. 6, pp. 1303–1309, Nov. 2005.

[52] J. Zeng, W. Qiao, L. Qu, and Y. Jiao, "An isolated multiport DC–DC converter for simultaneous power management of multiple different renewable energy sources," *IEEE J. Emerg. Sel. Topics Power Electron.*, vol. 2, no. 1, pp. 70–78, Mar. 2014.

[53] J. Zeng, W. Qiao, and L. Qu, "An isolated three-port bidirectional DC–DC converter for photovoltaic systems with energy storage," *IEEE Trans. Ind. Appl.*, vol. 51, no. 4, pp. 3493–3503, Jul. 2015.

[54] Y.-E. Wu and I.-C. Chen, "Novel integrated three-port bidirectional DC/DC converter for energy storage system," *IEEE Access*, vol. 7, pp. 104601–104612, 2019.

[55] S. S. Dobakhshari, S. H. Fathi, and J. Milimonfared, "A new soft-switched three-port DC/DC converter with high voltage gain and reduced number of semiconductors for hybrid energy applications," *IEEE Trans. Power Electron.*, vol. 35, no. 4, pp. 3590–3600, Apr. 2020.

[56] C.-L. Shen and L.-Z. Chen, "Dual-input isolated converter with dual-charge-pump cell for high step-up voltage ratio achievement," *IEEE Trans. Ind. Electron.*, vol. 67, no. 11, pp. 9383–9392, Nov. 2020.

[57] R. Kiran and R. Kalpana, "An isolated dual-input half-bridge DC–DC boost converter with reduced circulating power between input ports," *IEEE Can. J. Electr. Comput. Eng.*, vol. 45, no. 1, pp. 68–76, Winter. 2022.

[58] Y.-K. Tran, F. D. Freijedo, and D. Dujic, "Open-loop power sharing characteristic of a three-port resonant LLC converter," *CPSS Trans. Power Electron. Appl.*, vol. 4, no. 2, pp. 171–179, Jun. 2019.

[59] P. Wang, X. Lu, W. Wang, and D. Xu, "Hardware decoupling and autonomous control of series-resonance-based three-port converters in DC microgrids," *IEEE Trans. Ind. Appl.*, vol. 55, no. 4, pp. 3901–3914, Jul. 2019.

[60] D. Liu and H. Li, "A ZVS bi-directional DC–DC converter for multiple energy storage elements," *IEEE Trans. Power Electron.*, vol. 21, no. 5, pp. 1513–1517, Sep. 2006.

[61] L. Wang, Z. Wang, and H. Li, "Asymmetrical duty cycle control and decoupled power flow design of a three-port bidirectional DC–DC converter for fuel cell vehicle application," *IEEE Trans. Power Electron.*, vol. 27, no. 2, pp. 891–904, Feb. 2012.

[62] H. Tao, J. L. Duarte, and M. A. M. Hendrix, "Three-port triple-half-bridge bidirectional converter with zero-voltage switching," *IEEE Trans. Power Electron.*, vol. 23, no. 2, pp. 782–792, Mar. 2008.

[63] H. Tao, A. Kotsopoulos, J. L. Duarte, and M. A. M. Hendrix, "Triple-half-bridge bidirectional converter controlled by phase shift and PWM," in *Proc. 21st Annu. IEEE Appl. Power Electron. Conf. Expo.*, Mar. 2006, pp. 1256–1262.

[64] J. L. Duarte, M. Hendrix, and M. G. Simoes, "Three-port bidirectional converter for hybrid fuel cell systems," *IEEE Trans. Power Electron.*, vol. 22, no. 2, pp. 480–487, Mar. 2007.

[65] C. Zhao, S. D. Round, and J. W. Kolar, "An isolated three-port bidirectional DC–DC converter with decoupled power flow management," *IEEE Trans. Power Electron.*, vol. 23, no. 5, pp. 2443–2453, Sep. 2008.

[66] H. Tao, A. Kotsopoulos, J. L. Duarte, and M. A. Hendrix, "Transformer-coupled multiport ZVS bidirectional DC–DC converter with wide input range," *IEEE Trans. Power Electron.*, vol. 23, no. 2, pp. 771–781, Mar. 2008.

[67] Y. Wu, M. H. Mahmud, S. Christian, R. A. Fantino, R. A. Gomez, Y. Zhao, and J. C. Balda, "A 150-kW 99% efficient all-silicon-carbide triple-active-bridge converter for solar-plus-storage systems," *IEEE J. Emerg. Sel. Topics Power Electron.*, vol. 10, no. 4, pp. 3496–3510, Aug. 2022.

[68] S. Falcones, R. Ayyanar, and X. Mao, "A DC–DC multiport-converter-based solid-state transformer integrating distributed generation and storage," *IEEE Trans. Power Electron.*, vol. 28, no. 5, pp. 2192–2203, May 2013.

[69] P. Purgat, S. Bandyopadhyay, Z. Qin, and P. Bauer, "Zero voltage switching criteria of triple active bridge converter," *IEEE Trans. Power Electron.*, vol. 36, no. 5, pp. 5425–5439, May 2021.

[70] S. Dey and A. Mallik, "Multivariable-modulation-based conduction loss minimization in a triple-active-bridge converter," *IEEE Trans. Power Electron.*, vol. 37, no. 6, pp. 6599–6612, Jun. 2022.

[71] N. Naseem and H. Cha, "Triple-active-bridge converter with automatic voltage balancing for bipolar DC distribution," *IEEE Trans. Power Electron.*, vol. 37, no. 7, pp. 8640–8648, Jul. 2022.

[72] V. N. S. R. Jakka, A. Shukla, and G. D. Demetriades, "Dual-Transformer-Based asymmetrical triple-port active bridge (DT-ATAB) isolated DC–DC converter," *IEEE Trans. Ind. Electron.*, vol. 64, no. 6, pp. 4549–4560, Jun. 2017.

[73] E. S. Oluwasogo and H. Cha, "Self-current sharing in dual-transformer-based triple-port active bridge DC–DC converter with reduced device count," *IEEE Trans. Power Electron.*, vol. 36, no. 5, pp. 5290–5301, May 2021.

[74] I. Biswas, D. Kastha, and P. Bajpai, "Small signal modeling and decoupled controller design for a triple active bridge multiport DC–DC converter," *IEEE Trans. Power Electron.*, vol. 36, no. 2, pp. 1856–1869, Feb. 2021.

[75] K. Wang, W. Liu, and F. Wu, "Topology-level power decoupling three-port isolated current-fed resonant DC–DC converter," *IEEE Trans. Ind. Electron.*, vol. 69, no. 5, pp. 4859–4868, May 2022.

[76] Y.-M. Chen, Y.-C. Liu, and F.-Y. Wu, "Multi-input DC/DC converter based on the multiwinding transformer for renewable energy applications," *IEEE Trans. Ind. Appl.*, vol. 38, no. 4, pp. 1096–1104, Jul. 2002.

[77] M. I. Marei, B. N. Alajmi, I. Abdelsalam, and N. A. Ahmed, "An integrated topology of three-port DC–DC converter for PV-battery power systems," *IEEE Open J. Ind. Electron. Soc.*, vol. 3, pp. 409–419, 2022.

[78] B. N. Alajmi, M. I. Marei, and I. Abdelsalam, "A multiport DC–DC converter based on two-quadrant inverter topology for PV systems," *IEEE Trans. Power Electron.*, vol. 36, no. 1, pp. 522–532, Jan. 2021.

[79] H. Pinheiro and P. K. Jain, "Series-parallel resonant UPS with capacitive output DC bus filter for powering HFC networks," *IEEE Trans. Power Electron.*, vol. 17, no. 6, pp. 971–979, Nov. 2002.

[80] Y. Wang, F. Han, L. Yang, R. Xu, and R. Liu, "A three-port bidirectional multi-element resonant converter with decoupled power flow management for hybrid energy storage systems," *IEEE Access*, vol. 6, pp. 61331–61341, 2018.

[81] H. Krishnaswami and N. Mohan, "Three-port series-resonant DC–DC converter to interface renewable energy sources with bidirectional load and energy storage ports," *IEEE Trans. Power Electron.*, vol. 24, no. 10, pp. 2289–2297, Oct. 2009.

[82] Z. Lin, S. Pan, M. Wang, W. Lin, J. Gong, L. Yao, and P. Jain, "A three-port LCC resonant converter for the 380-V/48-V hybrid DC system," *IEEE Trans. Power Electron.*, vol. 37, no. 9, pp. 10864–10876, Sep. 2022.

[83] N. D. Dao, D.-C. Lee, and Q. D. Phan, "High-efficiency SiC-based isolated three-port DC/DC converters for hybrid charging stations," *IEEE Trans. Power Electron.*, vol. 35, no. 10, pp. 10455–10465, Oct. 2020.

[84] M. Forouzesh, Y. P. Siwakoti, S. A. Gorji, F. Blaabjerg, and B. Lehman, "Step-up DC–DC converters: A comprehensive review of voltage-boosting techniques, topologies, and applications," *IEEE Trans. Power Electron.*, vol. 32, no. 12, pp. 9143–9178, Dec. 2017.

[85] A. K. Bhattacharjee, N. Kutkut, and I. Batarseh, "Review of multiport converters for solar and energy storage integration," *IEEE Trans. Power Electron.*, vol. 34, no. 2, pp. 1431–1445, Feb. 2019.

[86] X. Pan, H. Li, Y. Liu, T. Zhao, C. Ju, and A. K. Rathore, "An overview and comprehensive comparative evaluation of current-fed-isolated-bidirectional DC/DC converter," *IEEE Trans. Power Electron.*, vol. 35, no. 3, pp. 2737–2763, Mar. 2020.

[87] N. Keshmiri, M. I. Hassan, R. Rodriguez, and A. Emadi, "Comparison of isolated bidirectional DC/DC converters using WBG devices for more electric aircraft," *IEEE Open J. Ind. Electron. Soc.*, vol. 2, no. 1, pp. 184–198, Jan. 2021.

[88] C. Zhang, J. Wang, K. Qu, B. Hu, Z. Li, X. Yin, and Z. J. Shen, "WBG and Si hybrid half-bridge power processing toward optimal efficiency, power quality, and cost tradeoff," *IEEE Trans. Power Electron.*, vol. 37, no. 6, pp. 6844–6856, Jun. 2022.

[89] H. Wouters and W. Martinez, "Bidirectional onboard chargers for electric vehicles: State-of-the-art and future trends," *IEEE Trans. Power Electron.*, vol. 39, no. 1, pp. 693–716, Jan. 2024.

[90] S. Hu, G. Liu, N. Jin, and L. Guo, "Model predictive current control for fault-tolerant bidirectional voltage source converter with open circuit fault and unbalanced grid voltage," *IEEE Access*, vol. 8, pp. 154966–154974, 2020.

[91] C. Cecati, A. O. Di Tommaso, F. Genduso, R. Miceli, and G. R. Galluzzo, "Comprehensive modeling and experimental testing of fault detection and management of a nonredundant fault-tolerant VSI," *IEEE Trans. Ind. Electron.*, vol. 62, no. 6, pp. 3945–3954, Jun. 2015.

[92] H. Tarzamni, F. P. Esmaeelnia, F. Tahami, M. Fotuhi-Firuzabad, P. Dehghanian, M. Lehtonen, and F. Blaabjerg, "Reliability assessment of conventional isolated PWM DC–DC converters," *IEEE Access*, vol. 9, pp. 46191–46200, 2021.

[93] M. Salimi, Y. Gong, S. Afrasiabi, X. Liang, and C. Y. Chung, "Power system resiliency studies under renewable energy penetration: A review," in *Proc. IEEE Can. Conf. Electr. Comput. Eng. (CCECE)*, Sep. 2022, pp. 429–434.

[94] H. Behjati and A. Davoudi, "Reliability analysis framework for structural redundancy in power semiconductors," *IEEE Trans. Ind. Electron.*, vol. 60, no. 10, pp. 4376–4386, Oct. 2013.

[95] M. S. Mahdavi, M. S. Karimzadeh, T. Rahimi, and G. B. Gharehpetian, "A fault-tolerant bidirectional converter for battery energy storage systems in DC microgrids," *Electronics*, vol. 12, no. 3, p. 679, Jan. 2023.

[96] S. Chakraborty, A. Chakrabarti, D. Maiti, and S. K. Biswas, "Transformer isolated fault tolerant three phase active front end converter for EV charging," *IEEE Trans. Transport. Electrific.*, vol. 10, no. 2, pp. 2332–2341, Jun. 2024.

[97] A. A. Gandomi, L. Parsa, K. A. Corzine, and V. Dargahi, "Fault-tolerant dual active isolated DC–DC converter," *IEEE Trans. Ind. Appl.*, vol. 59, no. 3, pp. 3565–3575, May 2023.

[98] L. Costa, G. Buticchi, and M. Liserre, "A fault-tolerant series-resonant DC–DC converter," *IEEE Trans. Power Electron.*, vol. 32, no. 2, pp. 900–905, Feb. 2017.

[99] P. Nachankar, H. M. Suryawanshi, P. Chaturvedi, D. Atkar, and V. V. Reddy, "Fault resilient soft switching DC–DC converter for modular solid state transformer applications," *IEEE Trans. Ind. Appl.*, vol. 58, no. 2, pp. 2242–2254, Mar. 2022.

[100] H. Wen, J. Li, H. Shi, Y. Hu, and Y. Yang, "Fault diagnosis and tolerant control of dual-active-bridge converter with triple-phase shift control for bidirectional EV charging systems," *IEEE Trans. Transport. Electrific.*, vol. 7, no. 1, pp. 287–303, Mar. 2021.

[101] K. Ambusaidi, V. Pickert, and B. Zahawi, "New circuit topology for fault tolerant H-bridge DC–DC converter," *IEEE Trans. Power Electron.*, vol. 25, no. 6, pp. 1509–1516, Jun. 2010.

[102] E. Pazouki, Y. Sozer, and J. A. De Abreu-Garcia, "Fault diagnosis and fault-tolerant control operation of nonisolated DC–DC converters," *IEEE Trans. Ind. Appl.*, vol. 54, no. 1, pp. 310–320, Jan. 2018, doi: 10.1109/TIA.2017.2751547.

[103] Z. Wang, Q. Luo, Y. Wei, D. Mou, X. Lu, and P. Sun, "Topology analysis and review of three-port DC–DC converters," *IEEE Trans. Power Electron.*, vol. 35, no. 11, pp. 11783–11800, Nov. 2020, doi: 10.1109/TPEL.2020.2985287.

[104] N. Zhang, D. Sutanto, and K. M. Muttaqi, "A review of topologies of three-port DC–DC converters for the integration of renewable energy and energy storage system," *Renew. Sustain. Energy Rev.*, vol. 56, pp. 388–401, Apr. 2016, doi: 10.1016/j.rser.2015.11.079.
[105] S. Sarani, H. Abootorabi Zarchi, and H. Delavaripour, "Ripple-free input current flyback converter using a simple passive circuit," *IEEE Trans. Ind. Electron.*, vol. 69, no. 3, pp. 2557–2564, Mar. 2022, doi: 10.1109/TIE.2021.3065624.
[106] S. Sarani, A. Nikbahar, H. A. Zarchi, and X. Liang, "An isolated high boost ratio DC–DC converter with very low input current ripples," *IEEE Trans. Circuits Syst. II: Exp. Briefs*, vol. 71, no. 9, pp. 4331–4335, Sep. 2024, doi: 10.1109/TCSII.2024.3386158.
[107] S. Sarani, H. A. Zarchi, and H. D. Poor, "A passive circuit to cancel input pulsating current of flyback converter," in *Proc. 11th Power Electron., Drive Syst., Technol. Conf. (PEDSTC)*, Tehran, Iran, Feb. 2020, pp. 1–5, doi: 10.1109/PEDSTC49159.2020.9088360.

**ALIREZA ASADI** was born in Kerman, Iran, in 1998. He received the B.S. degree in electrical engineering from the K. N. Toosi University of Technology, Tehran, in 2021, and the M.Sc. degree in electrical engineering from the University of Saskatchewan, Saskatoon, Canada, in 2024. In September 2024, he started working as an Engineer-in-Training (EIT) with the Interconnection Department, SaskPower, Regina, Canada. His research interests include multi-port and high-gain dc-dc converter, power electronics applications and renewable energy systems, resonant converters, and microgrids.

**XIAODONG LIANG** (Senior Member, IEEE) was born in Lingyuan, Liaoning, China. She received the B.Eng. and M.Eng. degrees in electrical engineering from Shenyang Polytechnic University, Shenyang, China, in 1992 and 1995, respectively, the M.Sc. degree in electrical engineering from the University of Saskatchewan, Saskatoon, Canada, in 2004, and the Ph.D. degree in electrical engineering from the University of Alberta, Edmonton, Canada, in 2013.

From 1995 to 1999, she was a Lecturer with Northeastern University, Shenyang. In October 2001, she joined Schlumberger (SLB), Edmonton, and was promoted to a Principal Power Systems Engineer with the world's leading oilfield services company, in 2009. She worked with Schlumberger for almost 12 years, until August 2013. From 2013 to 2019, she was with Washington State University, Vancouver, WA, USA, and the Memorial University of Newfoundland, St. John's, NL, Canada, as an Assistant Professor, and later an Associate Professor. In July 2019, she joined the University of Saskatchewan, where she is currently a Professor and Canada Research Chair in Technology Solutions for Energy Security in Remote, Northern, and Indigenous Communities. She was an Adjunct Professor with the Memorial University of Newfoundland, from 2019 to 2022. Her research interests include power systems, renewable energy, and electric machines.

Dr. Liang is a Registered Professional Engineer in the province of Saskatchewan, Canada, a fellow of IET, the Deputy Editor-in-Chief of IEEE TRANSACTIONS ON INDUSTRY APPLICATIONS, and the Co-Editor-in-Chief of IEEE CANADIAN JOURNAL OF ELECTRICAL AND COMPUTER ENGINEERING.

**SOBHAN SARANI** received the B.Sc. degree in electrical engineering from the University of Sistan and Baluchestan, Zahedan, Iran, in 2017, and the M.Sc. degree in electrical engineering from the Ferdowsi University of Mashhad, Mashhad, Iran, in 2020. From 2023 to 2024, he was a Research Assistant with the Power and Energy Conversion Laboratory, University of Saskatchewan, Saskatoon, Canada. His research interests include the design and control of power electronic converters, the modeling, analysis, and stability of grid integration of distributed and renewable energy resources, and grid-forming control of voltage source converters.

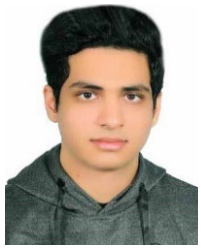

**MOHAMMAD SALEH KARIMZADEH** was born in Kerman, Iran. He received the B.S. degree in electrical engineering from the K. N. Toosi University of Technology, Tehran, Iran, in 2021, and the M.Sc. degree in electrical engineering from the Amirkabir University of Technology, Tehran, in 2024. His research interests include multi-port and high-gain dc-dc converter, power electronics applications and renewable energy systems, resonant converters, battery energy storage, and microgrids.